NASA/TM—1999–209478

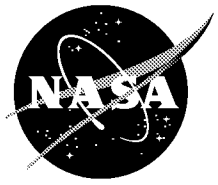

A Global Ocean Tide Model From TOPEX/POSEIDON Altimetry: GOT99.2

Richard D. Ray, Goddard Space Flight Center, Greenbelt, MD

National Aeronautics and
Space Administration

Goddard Space Flight Center
Greenbelt, Maryland 20771

September 1999

The NASA STI Program Office ... in Profile

Since its founding, NASA has been dedicated to the advancement of aeronautics and space science. The NASA Scientific and Technical Information (STI) Program Office plays a key part in helping NASA maintain this important role.

The NASA STI Program Office is operated by Langley Research Center, the lead center for NASA's scientific and technical information. The NASA STI Program Office provides access to the NASA STI Database, the largest collection of aeronautical and space science STI in the world. The Program Office is also NASA's institutional mechanism for disseminating the results of its research and development activities. These results are published by NASA in the NASA STI Report Series, which includes the following report types:

- TECHNICAL PUBLICATION. Reports of completed research or a major significant phase of research that present the results of NASA programs and include extensive data or theoretical analysis. Includes compilations of significant scientific and technical data and information deemed to be of continuing reference value. NASA's counterpart of peer-reviewed formal professional papers but has less stringent limitations on manuscript length and extent of graphic presentations.
- TECHNICAL MEMORANDUM. Scientific and technical findings that are preliminary or of specialized interest, e.g., quick release reports, working papers, and bibliographies that contain minimal annotation. Does not contain extensive analysis.
- CONTRACTOR REPORT. Scientific and technical findings by NASA-sponsored contractors and grantees.
- CONFERENCE PUBLICATION. Collected papers from scientific and technical conferences, symposia, seminars, or other meetings sponsored or cosponsored by NASA.
- SPECIAL PUBLICATION. Scientific, technical, or historical information from NASA programs, projects, and mission, often concerned with subjects having substantial public interest.
- TECHNICAL TRANSLATION. English-language translations of foreign scientific and technical material pertinent to NASA's mission.

Specialized services that complement the STI Program Office's diverse offerings include creating custom thesauri, building customized databases, organizing and publishing research results . . . even providing videos.

For more information about the NASA STI Program Office, see the following:

- Access the NASA STI Program Home Page at http://www.sti.nasa.gov/STI-homepage.html
- E-mail your question via the Internet to help@sti.nasa.gov
- Fax your question to the NASA Access Help Desk at (301) 621-0134
- Telephone the NASA Access Help Desk at (301) 621-0390
- Write to:
  NASA Access Help Desk
  NASA Center for AeroSpace Information
  7121 Standard Drive
  Hanover, MD 21076-1320

NASA/TM—1999–209478

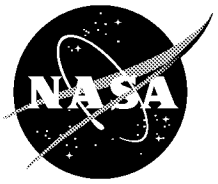

A Global Ocean Tide Model From TOPEX/POSEIDON Altimetry: GOT99.2

Richard D. Ray, Goddard Space Flight Center, Greenbelt, MD

National Aeronautics and
Space Administration

Goddard Space Flight Center
Greenbelt, Maryland 20771

September 1999

Available from:

NASA Center for AeroSpace Information
7121 Standard Drive
Hanover, MD 21076-1320
Price Code: A17

National Technical Information Service
5285 Port Royal Road
Springfield, VA 22161
Price Code: A10

Summary

Goddard Ocean Tide model GOT99.2 is a new solution for the amplitudes and phases of the global oceanic tides, based on over six years of sea-surface height measurements by the TOPEX/POSEIDON satellite altimeter. Comparisons with deep-ocean tide-gauge measurements show that this new tidal solution is an improvement over previous global models, with accuracies for the main semidiurnal lunar constituent M_2 now below 1.5 cm (deep water only). The new solution benefits from use of prior hydrodynamic models, several in shallow and inland seas as well as the global finite-element model FES94.1. This report describes some of the data processing details involved in handling the altimetry, and it provides a comprehensive set of global cotidal charts of the resulting solution. Various derived tidal charts are also provided, including tidal loading deformation charts, tidal gravimetric charts, and tidal current velocity (or transport) charts. Finally, low-degree spherical harmonic coefficients are computed by numerical quadrature and are tabulated for the major short-period tides; these are useful for a variety of geodetic and geophysical purposes, especially in combination with similar estimates from satellite laser ranging.

Contents

1 Introduction **1**

2 Altimeter Data Description and Data Processing **2**
2.1 Altimeter Corrections and Ancillary Data 2
2.2 Atmospheric Loading 3
2.3 Data Editing 5

3 Tidal Analysis of Altimetry **6**
3.1 Construction of Prior Model 7
3.2 Calculation of Load Tides 8
3.3 Harmonic Analysis of Binned Data 8

4 Model Tests **10**
4.1 Comparison with Tide Gauge Constants 10
4.2 Variance Reduction Tests 13

5 Spherical Harmonic Coefficients **16**

A Global Cotidal Charts **23**

B Global Ocean Loading Charts for M_2 **40**

C Global Charts of Tidal Transport Ellipses **52**

References **57**

Acknowledgments: I thank Brian Beckley for help with various aspects of the TOPEX/POSEIDON data processing. All altimeter data in this analysis are based on the Oceans Altimeter Pathfinder project (*Koblinksy et al.,* 1999). All figures in this document were created with the GMT plotting package, written by Paul Wessel (University of Hawaii) and Walter Smith (NOAA). The document itself was typeset with LaTeX 2_ε and *MathTime* fonts.

1 Introduction

The TOPEX/POSEIDON (hereinafter T/P) satellite was launched on August 10, 1992. Its two altimeters—the American TOPEX and French POSEIDON—have been working extremely well since the beginning of the mission, nearly seven years as of this writing. The mission's contribution to oceanography and geodesy has been impressive. Among the many publications describing important new findings, see especially the special issues of *Journal of Geophysical Research*, December 1994 and December 1995, as well as the mission's Internet homepage: `topex-www.jpl.nasa.gov`.

Within a year of launch the T/P mission brought about, *inter alia*, a burst of activity in global tidal modeling. The reason was twofold: (1) Its unprecedented accuracy allowed new global ocean tide solutions, even with only one year of data, which were far superior to any model of the tides then existing; (2) Analysis of the data for non-tidal signals depended crucially upon successful removal of the dominant tide signal, and this more than anything stimulated a great effort in tidal analyses. Some of the early tide solutions resulting from T/P data are described by *Le Provost, Bennett, and Cartwright* (1995). These solutions were extensively evaluated and compared by *Andersen et al.* (1995) and by *Shum et al.* (1997). See also the special issue of *Progress in Oceanography* (volume 40, 1997), which was devoted to the subject of ocean tides, including T/P results.

Since these early first-generation T/P results, new tidal models have continued to appear from time to time. The urgency of the early days has waned, and improvements are now of a more incremental nature. Most tidal investigators have been preoccupied with either applications of the new models or with dynamical interpretation of them, or with the study of secondary tidal signals in the T/P data, such as those from internal tides.

This report describes an updated solution for the global tides based on more than six years of T/P data. It too represents an incremental, but nonetheless clear, improvement to the earlier models. It builds primarily on the work of *Schrama and Ray* (1994, hereinafter SR94), and since there is now almost three times as much data available as SR94 used, the time for an update seems overdue. As in that work, the methodology is primarily one of empirical mapping, but with heavy reliance on a hydrodynamic prior model. My main purpose here is to document the solution for readers who may find the model useful, either for correcting altimeter data or for any of the myriad other possible applications. This report also provides a useful opportunity to present a large compilation of tidal charts, something that normally cannot be done in the established refereed literature but which many find useful for occasional reference. In addition, some readers may be unaware of the available products from such models (e.g., various load-tide charts or grids of global tidal

current velocities), and this report may help to publicize that.

The global tide model here described is dubbed GOT99.2 (the ".2" is needed to distinguish it from earlier versions that underwent a more limited release). The letters G, O, T nominally stand for Goddard Ocean Tide, but they might as well stand for Grenoble Ocean Tide, because, as will become apparent, this model relies heavily on the hydrodynamic model FES94.1, developed by Christian Le Provost's group, then at the Institut de Mécanique de Grenoble. The FES94.1 is the primary component in the prior model developed here, and it provides the complete tidal definition in polar latitudes above the T/P latitude limits. (In its reliance on the FES94.1 prior, our work is similar to the CSR3.0 and CSR4.0 models of Richard Eanes and to several other recent models.)

The main cotidal charts of the global tides resulting from this analysis of T/P altimetry are gathered together in Appendix A. Other related charts, such as those for ocean tidal loading, are in Appendices B and C. The main part of the report describes the analysis procedures that resulted in these solutions, plus a short section on model testing. There is also a section comprising tables of low-degree spherical harmonic coefficients from the global solutions; these are useful in many geophysical studies.

2 Altimeter Data Description and Data Processing

The tidal solution described here is based on 232 cycles (each cycle comprising data from 9.9156 days) of observations from both the TOPEX and the POSEIDON altimeters. The starting point was a special version of the Oceans Altimeter Pathfinder database (*Koblinsky et al.*, 1999), version 5.1 for T/P. This database has sea-surface height observations aligned at a fixed set of positions on the globe, with all necessary corrections applied according to the latest available information from the altimeter community. These corrections include various bias and drift corrections as established by the instrument engineers, as well as standard media corrections such as tropospheric delay. A few of these are worth mentioning in further detail because of the way they could potentially impact the ocean tide estimates.

2.1 Altimeter Corrections and Ancillary Data

The satellite ephemerides are those computed for the project by the Space Geodesy Branch at Goddard Space Flight Center (see, for example, *Marshall et al.*, 1995). The dynamical forcing from the Earth's gravitational field is modeled by JGM-3 (*Tapley et al.*, 1996). The dynamical forcing from the ocean tides is modeled by an early T/P altimeter tide solution described in an abstract by *Ray, Sanchez, and Cartwright* (1994), except that resonance terms (order-2 semidiurnals and order-1 diurnals), plus all long-period tides, are taken from the GEM-T3 gravity solution (*Lerch et al.*, 1992). Dynamical forcing from the body tide is according to *Wahr* (1981), which is compatible with that used for the ocean-tide solution in GEM-

T3. (In other words, any errors in the modeling of the body tide would have been absorbed into, and thus accounted for by, the GEM-T3 ocean tide solution.)

The body tide correction to the altimetry is equivalent to that selected and employed by the T/P project. It is therefore equivalent to that used in nearly all other T/P tidal analyses. The correction is based on the Cartwright-Tayler-Edden harmonic expansion of the tidal potential (*Cartwright and Edden,* 1973), extrapolated to the 1990-2000 epoch (using the time dependence evident in their tables from tabulated epochs 1870, 1924, and 1960). While newer potential expansions are now available (they are used mostly for Earth-tide studies), there is no reason to believe that the C-T-E potential is inadequate for present purposes. The adopted h_2 and h_3 Love numbers, required for computing the body tide, are roughly those of *Wahr* (1981). They assume the body tide is perfectly elastic. For all tides of degree 2, independent of frequency, h_2 is taken as 0.609, except that K_1 and its nodal sidelines are taken as 0.52. Some newer computations of the Love numbers differ significantly from these values, and, as is well known, the behavior of h_2 at frequencies surrounding the nearly diurnal free wobble is more complex than that given by the single adjustment to K_1 (as, in fact, Wahr's work showed). Finally, all latitude dependence in Love numbers (admittedly small) has been ignored in the body-tide correction. Any errors caused by these limitations in the Love numbers, or in the body tide generally, will be directly absorbed into the estimated ocean tides. This point should be kept in mind for certain specialized applications of the altimeter-based tide models. (For completeness, the degree-3 tide corrections use $h_3 = 0.291$. So far as I'm aware, no altimeter solutions have been attempted for degree-3 tides.)

The other component of the solid-Earth tide, namely the load tide, is handled as part of the altimeter ocean tide solution, as discussed below.

The ionospheric delay correction is of some interest because of the strong solar periodicity in it and its potential corruption of the solar ocean tide estimates. It is thought to be one reason why the older GEOSAT tide solution of *Cartwright and Ray* (1990) was less accurate in its S_2 solution, there having been only a very poor ionospheric correction available for GEOSAT. This problem is much reduced for TOPEX, of course, because of its two-frequency altimeter. For POSEIDON, the correction is based on a model tuned by observations from DORIS ranging to T/P. While not as accurate as TOPEX it is still much superior to that used on GEOSAT. (In any event, POSEIDON accounts for only about 10% of the total T/P altimetry.)

In this "special version" of the Pathfinder database (kindly created by Brian Beckley) no corrections were applied for ocean tides, load tides, or atmospheric loading. The reason for the lack of tide corrections is obvious; the handling of atmospheric loading is described next.

2.2 Atmospheric Loading

The loading of the ocean by the atmosphere is a large source of variability in sea level, as is well known. For any tidal analysis of altimeter data, it is almost mandatory that this large source of "noise" be removed. The traditional way to do this is

by applying an isostatic inverted barometer correction, although some recent work (e.g., *Stammer et al.*, 1999) explores a more dynamically based correction. Since tides are generally aliased by the satellite sampling into long periods where the inverted barometer response of the ocean is known to hold fairly well, this approximation is generally adequate for tides.

The T/P data supplied by the project office contains (or originally contained) no explicit loading correction or atmospheric pressure estimate, so most users of the data have applied an inverted barometer correction by deducing sea-surface pressure from the supplied dry-troposphere correction. These pressure data are based on a slightly modified version of the operational weather products from the European Centre for Medium-range Weather Forecasting (ECMWF), provided at six-hour intervals. For tidal studies this is problematic because the ECMWF surface pressures are known to contain atmospheric tide signals (*Hsu and Hoskins*, 1989), the dominant ones being S_2 (about 1.2 mbar at the equator) and S_1 (geographically variable but generally smaller than S_2, especially over the ocean). This is problematic for three reasons:

1. The ocean's response at the S_1 and S_2 periods is certainly not isostatic. If it were, then the short-period ocean tides could similarly be described by an equilibrium tide model, which is patently not the case. Therefore, applying an IB correction at these periods is adding, not removing, noise from the data. Moreover, it is adding noise at the tidal periods, directly contaminating the ocean tide estimates.

2. No matter how the ocean responds to atmospheric tidal forcing, we have traditionally considered this response to be part of the ocean tide—its "radiational" component (*Munk and Cartwright*, 1966; *Cartwright and Ray*, 1994). We wish to map this, not remove it.[1]

3. The six-hourly sampling of the pressure is at the Nyquist period for S_2, so in fact the S_2 air tide is only partially in the supplied pressures. At some longitudes the full tidal signal is there, at other longitudes it is completely missing.

Point (3) could, of course, be solved by obtaining more rapid pressure data, assuming that such data exist and that they accurately simulate the atmospheric tides (not signals that most GCM developers are interested in). But points (1) and (2) suggest

[1]Non-traditionalists may argue that it may be useful to remove the radiational component of the tide, perhaps in the manner that *Stammer et al.* (1999) describe, and to let our tidal analyses map simply the gravitational part of the tide. This is a valid argument. But it implies that the dynamical model used to remove the pressure-driven ocean variability has great skill at tidal periods (and that the forcing pressures are adequately known). I submit that experience with purely numerical tidal models suggests that this skill is not high, and that it is therefore preferable to let the altimetry empirically determine the full (gravitational + radiational) tide. Otherwise we are left with a gravitational part of the tide, distorted by the errors in the pressure-driven model. While many users of altimetry would not care about this so long as the signal is gone, Earth scientists who need a good tide model would care.

that another approach is needed. Several years ago (in an incompetently typeset T/P project report) I gave an algorithm that attempted to remove the S_2 signal from the project-supplied pressure data, to be used before tidal analysis is undertaken. That algorithm was only a stopgap measure, its main advantage being that it was very easy to use. In this work, another approach is adopted.

For its simplicity and its validity at periods greater than several days, the inverted barometer approximation has been retained. However, to avoid applying this approximation at short periods, and especially to avoid doing so at tidal periods, new pressure data have been obtained in the form of daily means. Such data are readily available over the Internet from the U. S. National Center for Environmental Prediction (NCEP) for the entire T/P duration. These data obviously have no signals at S_2 or S_1, and they have by necessity reduced variability at all periods below several days.

On a related point, note that the dry tropospheric correction is preferably based on the original pressure data—in fact, 3-hour data would be even more desirable. In this correction the full tidal signal is desired, since it represents a real delay error from the atmosphere. The S_2 component in the dry-tropospheric correction is about 2.6 mm amplitude at the equator, so generally this component is small, but at certain longitudes in the tropics, the unfortunate Nyquist pressure sampling will cause an error in our S_2 of this full 2.6 mm. There is no similar error at S_1, at least to the extent that the ECMWF pressures adequately model S_1.

Although the above discussion may seem overly detailed and involved, careful handing of these effects is essential if one is to study the radiational tide in the manner of *Cartwright and Ray* (1994). Such studies are anticipated from the present solutions.

2.3 Data Editing

The processing of altimetry has now become so routine that most papers on the subject hardly bother describing such mundane details as data editing. Since I have unlimited space here, I take the opportunity to describe briefly some of these details for the present processing. Many aspects of the data handling and editing were set up early in the mission and have hardly been considered since then. Some of them could profitably be revisited now that a substantial altimeter dataset exists. Thus, the following criteria simply document what was done; they are not meant to act as general recommendations for other users.

The Ocean Pathfinder data that we use have already been cleaned up and edited to a great extent. Much of this work is described in *Koblinsky et al.* (1999). Some of the primary data editing ensures that necessary corrections fall within acceptable ranges; these include significant wave height (which determines sea-state bias), wet and dry troposphere corrections, and the ionosphere correction (which must be smoothed along-track before being applied). These checks are applied before Pathfinder users obtain the data. Further details are in the Pathfinder report.

Additional to these checks (and some simplistic ones not worth mentioning), data are here rejected if:

1. The location of the observation falls in a region of high geoid gradient and also deviates by more than 1 km from the reference satellite groundtrack.

2. The standard deviation of a 1-s average height (formed from 10-Hz data) exceeds 15 cm. This criteria was once thought to be a useful check of rain-contaminated data. It is probably set too low for POSEIDON data, since proportionally more of these data were rejected than for TOPEX.

3. The significant wave height exceeds 10 meters, since the sea-state bias correction is then suspect.

4. The Automatic Gain Control (AGC) for the TOPEX Ku altimeter falls outside the range [28, 40] dB while in high latitudes. High AGC would suggest possible sea ice in the altimeter footprint. A check on AGC in low latitudes must be done more carefully, because near-specular returns have sometimes been seen for apparently good data, especially in inland seas.

5. The observed sea level, after correcting for atmospheric loading and for tides (with the prior model—see below), differs from mean sea level at that location by 50 cm or more. This test is applied only in deep water.

6. The observed sea level falls outside a 4-σ interval for all other altimeter measurements at that location during the mission.

Criteria 1–4 deleted 0.23% of all observations. Criterion 5 deleted 0.56%, and criterion 6 deleted 0.03%. Thus only 0.82% of the data were deleted. Note that no check is done on attitude; the project-recommended test set at 0.45° from nadir was found to cause an inordinate number of deletes of apparently good data.

3 Tidal Analysis of Altimetry

In briefest terms the altimeter processing performed here involves gathering all observations surrounding each point on the globe and determining an empirical adjustment to a prior tide model. The steps taken are as follows:

1. Construct a prior model of the global ocean tides and compute the corresponding load tide. Together these provide the prior model for correcting altimeter observations for tidal variations.

2. At each grid location of the prior model, gather all 'nearby' altimeter observations and apply tidal corrections according to the prior model (as well as corrections for atmospheric loading, as discussed above).

3. Perform tidal analysis of these residuals.

4. Extend the computed tidal adjustments into regions lacking sufficient altimetry by interpolation or extrapolation. For extrapolation (especially into polar oceans) use a smooth taper toward zero adjustment.

5. If necessary, smooth the extended adjustments. (This is most necessary for small, hence noisy, constituents like Q_1.)

6. Add the tidal adjustment to the prior model to determine a new ocean + load model.

7. Compute a new load tide from this model and remove it to form a new model of the global ocean tide.

Some of these steps will now be described in greater detail.

3.1 Construction of Prior Model

From previous experience it appears to be of considerable benefit to use a prior, or starting, model of the ocean tides, especially a hydrodynamic model that is capable of capturing shorter wavelength features of the tide that the relatively widely spaced altimeter tracks cannot map. This is the procedure that *Schrama and Ray* (1994) and a number of other groups took in their analyses. One of the benefits of this approach, which was especially useful early in the mission, is that it makes handling any tidal aliasing problems much easier (see SR94 for an extensive discussion of aliasing in the T/P data). When the altimetry is used to map essentially the long-wavelength part of the tidal field, then data from several ground-tracks can be combined simultaneously in the tidal analysis; the additional phase observations so obtained considerably reduce most aliasing problems.

The prior ocean-tide model used here is primarily the FES94.1 model of *Le Provost et al.* (1994). The same prior model was used in the SR95 and CSR3.0 solutions. The one serious drawback of this model for the present purpose, described in detail by *Smith and Andersen* (1997), is a subtle boundary error caused by the way the global model was constructed from a series of basin-wide solutions. In the elevations this error is hardly noticeable, but in inferred tidal currents (and in energy-flux divergences) it is more apparent. Nonetheless, the FES94.1 model was still adopted because it appears to be still the best available. (A later assimilation model from the Grenoble group, FES95.2 (*Le Provost et al.*, 1998), has some difficulties in near-coastal waters, although it is better in deep water.) The FES94.1 model is available on a global 0.5° grid, including the Arctic Ocean and the Ross and Weddell Seas.

The FES94.1 model has been supplemented here by the following local tide models:

- *Canceil et al.* (unpublished) – Mediterranean Sea.
- *Lambert et al.* (1998) – Gulf of Maine and Gulf of St. Lawrence.
- *Proctor et al.* (1994) – Persian Gulf.
- *Ray and Egbert* (unpublished) – Red Sea.

The unpublished Red Sea model is an assimilation solution, based on along-track T/P data; it was computed using the Oregon State Tidal Inversion Software (OTIS, written by Gary Egbert and Lana Erofeeva). The Gulf of Maine model is based in part on earlier calculations by *Greenberg* (1979).

The spatial resolutions of these local models vary from 0.25° (Gulf of Maine) to 5′ (Persian Gulf and Red Sea). For merging with the primary FES94.1 model, these local models were resampled at 0.5°, which sacrifices their fine spatial resolutions but offers convenience and ease of final use. Merging of the local models into the global model is then straightforward for most, because the gulfs and inland seas are generally separated from the global ocean by narrow straits where a clean break can be placed. The Gulf of Maine model is more problematic; it was merged by using a tapered weighted averaging in the region of overlap between it and FES94.1. This merger is not evident by eye, but any detailed analysis could likely find artifacts of it.

The tidal prediction software necessary for applying the prior tide model to altimeter data is the same as that distributed with the GOT99.2 datasets (called `perth2`). It accounts for short-period (diurnal and semidiurnal) tides and includes 26 constituents, the minor ones being inferred from the major ones by admittance relationships.

3.2 Calculation of Load Tides

According to the steps outlined above, the estimates of the radial displacement load tide are required—first, to determine the prior ocean + load model, and second, to determine the final model from the adjusted ocean + load model. In both cases, a spherical harmonic approach has been used, as described in Appendix A of *Cartwright and Ray* (1991). In theory, computation of the load tide from the ocean + load tide requires iteration, but the iteration is so rapid that one iterative step is sufficient.

In keeping with the 0.5° global grid, spherical harmonic expansions are computed to degree and order 360. The required loading Love numbers h'_n for $n = 1, \ldots, 360$, are from *Farrell* (1972). They are taken to be real (not complex) numbers; i.e., like the body tide the load tide is assumed to be perfectly elastic. The computed load tide appears to be quite insensitive to possible small errors in h'_n. Further discussion of load tides, including quantities other than radial displacement, may be found in Appendix B.

3.3 Harmonic Analysis of Binned Data

For the tidal analysis at each position over the 0.5° grid, data are accumulated into overlapping bins. As in SR94 the size of these bins in the deep ocean is large enough to capture data from at least two descending and two ascending tracks. This size was required in SR94 to avoid the most severe tidal aliasing problems with the relatively short time series. While the time series is now much longer, allowing in principle smaller bin sizes, the harmonic analysis is now extended to include more

constituents. This extension benefits from having data from at least four tracks, and the results from SR94 suggest that the possible loss of spatial resolution was not a limiting factor in deep water. In shallow water the adopted bin sizes are allowed to decrease, to an extent that in theory the analysis may rest on data from only one track, although this rarely happened. The bins are always taken sufficiently large to average data along at least 150 km of a given track in order to average out possible surface effects of internal tides (*Ray and Mitchum*, 1997).

Cartwright and Ray (1990) showed the many advantages of a response type of tidal analysis when applied to satellite altimeter data. However, in the present work, as in SR94, a harmonic method has been employed. This is partly to continue the heritage of SR94-type solutions. More importantly, however, it allows the fine structure of the tidal admittances across each band to be explored on a global scale. This includes admittance fine structure from radiational effects (e.g., *Cartwright and Ray*, 1994), as noted above. The use of harmonic methods is also consistent with the adopted prior model, which may not have errors satisfying a smooth admittance assumption.

In the GOT99.2 solution the following constituents were solved for: Sa, Ssa, Mf, Q_1, O_1, P_1, S_1, K_1, N_2, M_2, S_2, K_2. Of these tides, the most severe aliasing problems occur for Ssa and K_1 and for P_1 and K_2; both of these require in principle at least nine years of data for clean separation, given only data at one location (SR94). (In fact, the Ssa/K_1 aliasing is more problematic because of the typically wide spectral width of Ssa, reflecting its primarily weather-driven forcing.) While 232 cycles of T/P comprise less than nine years of data, the addition of data from neighboring tracks somewhat helps to reduce both aliasing problems.

Several groups have already published studies of the Sa and Ssa elevations deduced from T/P, so these results will not be described here. (Moreover, they are normally not included as part of the "tide correction" in altimetry, nor are they normally employed in gravity and loading corrections because much of their elevation signal is steric.) The small constituents Mf and S_1 require some additional steps for noise reduction; these results will be addressed elsewhere. This report thus concentrates on the eight remaining short-period tides.

The solution for the above listed constituents is found by least squares from the accumulated data at each grid position. Nodal modulations are, of course, applied to all lunar tides; these are updated every 30 days as required. These solutions, representing required adjustments to the prior tide model, are then interpolated or extrapolated into regions lacking altimetry, as noted above, smoothed as necessary, and added to the prior model. The smoothing is different for each constituent, small minor tides being more easily corrupted by noise and therefore in need of greater smoothing. The smoothing has also been reduced in shallow water where rapid variations in the tide are to be expected. After computation and removal of the radial-displacement load tide, the final constituent grids are obtained. The valid data cover the exact regions where the prior model was defined, which is nearly the entire globe. High-latitude regions, polewards of about 73°, are defined completely by the FES94.1 hydrodynamic model. All regions polewards of the T/P limit 66°

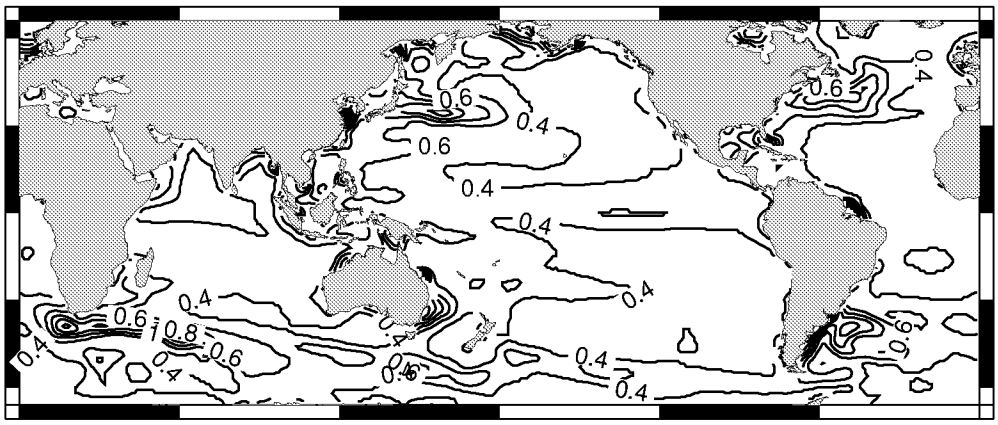

Figure 1: Standard errors for M_2 estimates. Contour interval = 0.2 cm

are necessarily less accurate than elsewhere on the globe.

Figure 1 shows the standard errors for the least squares estimated adjustments to M_2. These are according to the covariance matrix computed for each binned solution and have been scaled (a) by the estimated noise based on the standard deviation of the final residuals and (b) by a scalar factor that approximately accounts for serial correlation along individual tracks in each bin. According to these estimates, the standard error for M_2 thoughout most of the deep ocean is of order 0.5 cm. Near strong western boundary currents and other sources of significant mesoscale variability the tidal errors are understandably larger. Any correlated errors not accounted for (e.g., correlations between different tracks caused by errors in the ionospheric delay) would inflate these error estimates. The errors also do not account for inherent temporal variability in the M_2 tide itself, variability discussed, for example, by *Munk et al.* (1965) and *Ray and Mitchum* (1997), which can exceed 1 cm even in the open ocean. Some independent determination of reliabilty of the tidal estimates is therefore necessary, to which we now turn.

4 Model Tests

Two kinds of tests of the GOT99.2 tide solution are reported in this section. One test uses comparisons with a standard set of deep-ocean tide gauges, the other uses variance reduction calculations along a few selected T/P tracks in near-coastal and shallow water. Many other tests might be performed, including some employed by *Shum et al.* (1997), but these two tests suffice to establish that the present solution does appear to be an advancement over earlier global models.

4.1 Comparison with Tide Gauge Constants

This section adopts exactly the same set of 102 tide gauge stations used by *Shum et al.* (1997) in their comprehensive comparisons of about a dozen global ocean tide models. These stations are either bottom pressure recorders located in the deep

ocean or conventional gauges located at small, relatively isolated islands. They are thus designed to test the deep-ocean accuracy of models. Such gauge comparisons also test the efficacy with which the solid tide has been removed from altimeter measurements. Although a couple of the stations now look somewhat suspect (perhaps owing to very local influences), it is desirable to maintain consistency with the Shum et al. tests and hence to use the same comparison dataset.

Table 1 gives a detailed comparison for the present M_2 solution, showing for each tide gauge the amplitude H and phase lag G for the gauge and for the altimeter estimate and their inphase $H1$ and out-of-phase $H2$ difference (in cm). All stations labeled "IAPSO" are bottom pressure stations numbered and compiled originally by David Cartwright for IAPSO. Most, but not all, of the remaining stations are island tide gauges.

Table 1: Tide gauge comparisons for M_2.

			Tide Gauge		GOT99.2		Difference (cm)	
Station	Position		H	G	H	G	$H1$	$H2$
IAPSO.1.1.30	60.2	331.2	69.6	183.0	69.6	183.8	.0	-.9
IAPSO.1.1.71	57.2	349.9	102.9	169.0	101.2	167.8	2.2	1.8
IAPSO.1.2.63	54.0	307.2	39.9	295.0	40.4	296.4	1.1	-.1
IAPSO.1.1.35	53.6	346.1	98.3	142.0	96.8	142.6	.6	-1.7
IAPSO.1.1.33	53.5	334.9	52.6	145.0	52.4	145.7	-.2	-.6
IAPSO.1.2.36	44.5	319.5	14.7	31.0	14.5	31.2	-.2	-.1
IAPSO.1.1.40	41.4	332.0	46.7	73.0	46.6	72.6	.3	-.2
IAPSO.1.1.74	40.3	345.0	88.0	74.0	85.2	73.6	-.2	-2.9
Flores Island	39.5	328.9	38.2	59.0	37.5	56.6	1.0	-1.4
IAPSO.1.2.101	37.8	292.0	42.1	353.0	41.7	353.3	-.4	.3
IAPSO.1.1.41	37.2	339.9	66.3	63.0	66.9	62.4	.9	.3
IAPSO.1.1.72	34.0	330.6	36.7	43.0	36.3	43.0	-.3	-.3
IAPSO.1.2.38	33.9	318.8	25.7	10.0	26.0	11.1	.2	.5
Funchal	32.6	343.1	72.1	46.0	72.2	45.6	.4	-.3
St George	32.4	295.3	35.7	358.0	35.8	355.9	.0	-1.3
IAPSO.1.2.15	28.5	283.2	40.8	2.0	39.9	2.5	-.9	.3
IAPSO.1.2.5	28.2	292.5	34.0	359.0	32.3	359.3	-1.8	.2
IAPSO.1.2.39	26.6	316.0	15.0	329.0	15.0	330.4	.2	.3
IAPSO.1.2.9	26.5	290.7	31.7	.0	31.1	1.8	-.6	1.0
IAPSO.1.2.6	24.8	270.4	1.3	226.0	.9	212.4	.1	.4
PRAIA 85	14.9	336.5	38.9	248.4	39.8	246.6	-1.5	-.4
IAPSO.1.3.13	14.7	311.2	32.9	233.0	35.1	232.5	-1.5	-1.5
IAPSO.1.3.15	7.0	308.5	57.3	222.0	55.4	222.3	1.6	1.1
IAPSO.1.3.8	.9	330.7	71.7	212.0	72.2	212.9	.2	-1.2
IAPSO.1.3.19	.2	318.8	86.9	219.0	86.0	219.2	.9	.3
IAPSO.1.3.16	.0	340.0	55.1	204.0	55.0	204.4	.3	-.3
IAPSO.1.3.17	.0	350.0	33.5	160.0	33.0	159.5	.7	.1
Annobon Island	-1.4	5.6	50.0	94.0	50.5	93.3	.6	.5
Fernando	-3.8	327.6	80.9	206.0	79.4	207.0	1.9	-.6
Ascension Is.	-7.9	345.6	33.1	178.0	33.8	176.9	-.6	.7
Jamestown	-15.9	354.3	32.0	80.0	32.3	77.4	1.5	.0
IAPSO.1.3.10	-17.1	346.3	16.1	137.0	15.9	138.7	-.2	-.5
IAPSO.1.3.11	-18.0	323.9	53.7	185.0	55.7	183.2	-2.2	1.6
Ilha de Trindad	-20.5	330.7	39.8	188.0	39.5	187.9	.3	.1
IAPSO.1.4.23	-38.5	348.9	25.5	11.0	26.3	10.6	.8	.0
IAPSO.1.4.5	-53.5	303.0	36.0	281.0	35.3	280.0	-.8	.6
King Edward	-54.3	323.5	24.4	274.4	24.1	279.3	2.0	.6
IAPSO.1.4.1	-54.5	3.3	14.5	21.0	15.1	22.3	.5	.6
IAPSO.4.2.21	-56.5	297.0	43.3	265.0	40.8	261.6	-2.2	2.7
IAPSO.4.2.8	-56.7	307.5	39.8	274.0	39.2	272.9	-.8	.5
IAPSO.4.2.18	-60.0	312.9	41.7	268.0	42.0	269.0	.7	-.4
IAPSO.4.2.24	-61.5	298.7	32.5	268.0	32.4	273.8	3.3	.2

continued from previous page

Station	Position		Tide Gauge		GOT99.2		Difference (cm)	
			H	*G*	*H*	*G*	*H*1	*H*2
IAPSO.3.2.1	4.2	52.9	32.2	34.0	31.6	33.9	-.4	-.4
Hulule	4.2	73.5	23.6	226.4	23.0	229.9	1.4	-.5
Gan	-.7	73.2	30.0	250.5	29.5	250.2	.0	.5
Port Victoria	-4.6	55.5	40.4	13.5	44.7	14.6	4.0	1.9
Aldabra	-9.4	46.2	93.0	23.0	92.1	22.5	-.5	-1.1
Christmas Is.	-10.4	105.7	35.5	8.5	36.4	9.1	.9	.5
Aaglega Is.	-10.4	56.7	28.7	350.1	29.7	352.3	1.2	1.0
Cocos Island	-12.1	96.9	30.7	312.9	30.6	309.1	-1.5	-1.3
Dzaoudzi	-12.8	45.3	104.4	26.4	105.8	25.4	2.1	-1.0
Rodrigue	-19.7	63.4	38.4	255.4	39.3	252.4	-2.2	-.3
Port Louis	-20.2	57.5	15.1	269.4	19.0	265.7	-1.3	-3.9
IAPSO.3.2.16	-28.3	66.8	41.1	238.0	41.3	237.5	-.5	.0
IAPSO.4.1.1	-37.0	132.0	14.2	64.0	14.8	72.6	-1.8	1.4
Amsterdam Is.	-37.9	77.6	40.7	229.6	40.3	229.8	.3	.2
IAPSO.4.1.2	-50.0	132.1	12.3	65.0	11.5	64.9	-.3	-.7
Heard Is.	-53.0	73.4	24.0	191.0	21.3	190.7	2.6	.6
IAPSO.4.1.3	-60.0	132.1	18.5	79.0	18.7	76.2	.9	.0
IAPSO.2.1.32	59.1	184.9	22.8	106.0	23.8	101.5	1.5	1.4
IAPSO.2.1.17	56.1	215.6	97.1	283.0	96.3	281.8	-2.1	.3
IAPSO.2.1.52	53.4	205.7	73.3	298.0	72.4	298.9	.5	1.4
IAPSO.2.1.16	53.3	224.4	99.7	267.0	99.7	264.4	-4.5	.4
Massacre Bay	52.8	173.2	21.5	95.6	22.0	96.3	-.3	.5
IAPSO.2.1.15	49.6	227.2	90.5	252.0	90.4	251.5	-.7	.4
IAPSO.2.1.1	46.8	229.2	80.5	241.0	81.5	241.7	.4	-1.4
IAPSO.2.1.39	43.3	199.9	35.0	300.0	34.9	299.6	-.3	.0
IAPSO.2.1.43	40.7	190.6	19.2	327.0	19.3	320.2	-1.2	-2.0
IAPSO.2.1.42	36.5	196.0	20.8	309.0	20.7	309.0	-.1	.1
IAPSO.2.1.25	33.5	225.8	25.5	220.0	23.7	221.0	1.6	.9
IAPSO.2.2.1	32.0	149.8	13.9	191.0	13.0	192.1	.9	-.1
Midway	28.2	182.6	11.7	93.7	10.7	89.6	.8	-1.0
Chichijima	27.1	142.2	28.0	262.2	22.9	261.7	.5	5.1
IAPSO.2.1.31	25.0	226.1	14.8	85.0	12.2	85.4	-.3	-2.5
Marcus Island	24.3	154.0	7.6	152.1	8.2	143.6	.2	1.3
French Frigate	23.9	193.7	9.2	58.4	11.4	56.2	1.5	1.7
IAPSO.2.3.1	21.5	250.1	38.9	95.0	36.9	98.3	-1.9	-2.3
Wake	19.3	166.6	27.9	116.2	28.8	116.1	-.4	.8
IAPSO.2.3.2	18.9	207.5	25.0	33.0	23.5	33.4	-1.3	-.7
Isla Socorro	18.7	249.0	33.1	98.6	35.3	96.9	.7	2.3
Johnston	16.7	190.5	26.2	101.3	25.9	101.4	.0	-.3
Saipan	15.2	145.7	17.8	294.8	15.6	290.0	-2.2	1.6
Yap Is.	9.5	138.1	41.0	294.0	42.9	293.5	.4	-1.9
Majuro	7.1	171.4	52.7	130.9	52.5	128.9	1.6	1.0
Ponape	7.0	158.2	27.7	128.2	28.7	124.0	1.1	2.0
Christmas Is.	2.0	202.5	26.7	81.4	27.5	72.2	4.4	-.2
Betio	1.4	172.9	58.8	139.5	58.3	136.6	2.3	1.9
Galapagos	-.4	269.7	72.6	246.1	72.2	243.2	-3.1	1.9
Seeadler Harbor	-2.0	147.3	8.9	272.7	8.3	277.2	.6	.6
IAPSO.2.3.4	-2.9	265.0	40.9	245.0	40.2	244.7	.1	.7
Funafuti	-8.5	179.2	55.7	154.8	57.3	153.9	-1.0	1.4
Nuku	-8.9	219.9	48.5	30.3	48.5	29.2	.4	-.8
Pago Pago	-14.3	189.3	36.6	179.0	38.2	174.6	-1.5	3.0
Papeete	-17.5	210.5	7.7	305.7	7.0	324.8	1.3	2.2
Vila BHI	-17.8	168.3	36.9	205.5	36.8	196.7	-2.0	5.3
Raratong	-21.2	200.2	25.8	209.2	25.9	210.2	.2	-.4
Rikitea	-23.1	225.1	27.5	348.4	26.9	350.2	-.4	1.0
Easter Island	-27.2	250.6	20.9	15.8	19.5	13.0	-1.1	-1.3
Kingston	-29.1	167.9	57.2	264.2	53.1	261.4	-2.1	4.4
Lord Howe I.	-31.5	159.1	59.0	304.2	60.3	301.1	-2.0	-2.7
Robinson Crusoe	-33.6	281.2	31.5	66.1	33.6	69.4	-.9	2.7
Macquarie I.	-54.5	159.0	29.6	28.4	32.1	27.4	2.5	.7

Table 2 gives the rms discrepancies between each listed model and the tide-gauge harmonic constants for each of the eight major short-period constituents. The listed models include the present GOT99.2 solution, plus several of the models from the Shum paper that showed the best comparisons, and the recently released model CSR4.0 from Richard Eanes (University of Texas). Note that the prior model used in the present work has an rms discrepancy in M_2 of 2.87 cm, which is reduced in the new solution to 1.47 cm.

It is reassuring that the new GOT99.2 solution does show an improved agreement with the tide gauges for all eight constituents. (One wonders how low these statistics can get, given the inherent errors in the tide gauge data.) The smallest improvement is apparently in Q_1. Table 2 reflects, however, only an average deep-water test, and it turns out that the largest adjustment to the Q_1 prior model occurs in the Sea of Okhotsk (known for its large diurnal tides). So at least in one region there is likely to be significant improvement even in Q_1 although Table 2 will not reflect it.

One interesting minor point concerning Table 2 is that the models showing the largest discrepancies in the K_2 tide (i.e., the models by Desai and Wahr and by Eanes) employ the simplified response method that *Cartwright and Ray* (1990) used with GEOSAT data. This method does not account for the "jerk" in the semidiurnal admittance at S_2, caused primarily by the S_2 radiational tide. These response-type solutions might therefore benefit from either an additional radiational potential (*Cartwright and Tayler*, 1971) or from the S_2 radiational adjustment advocated by *Cartwright and Ray* (1994). The reason why such an adjustment would improve primarily K_2 is that the S_2 tide is so strong in T/P data that the admittance is always forced to fit it; the fit must therefore be sacrificed at the smaller nearby K_2.

4.2 Variance Reduction Tests

It is beyond the scope of the present work to perform a comprehensive set of variance reduction tests in altimeter collinear and/or crossover data. (In any event, such tests are being done by other groups [Patrick Vincent, SWT Keystone meet-

Table 2: Tidal RMS comparisons to 102 "ground-truth" stations (cm)

Authors	version	Q_1	O_1	P_1	K_1	N_2	M_2	S_2	K_2
Desai-Wahr	3.2.78	0.34	0.98	0.42	1.28	0.70	1.85	1.09	0.56
Le Provost *et al.*	FES95.1	0.29	1.04	0.45	1.22	0.83	1.65	1.00	0.48
Ray *et al.*	941230	0.37	0.99	0.39	1.26	0.78	1.89	1.18	0.49
Eanes	CSR3.0	0.30	0.95	0.40	1.12	0.67	1.64	1.03	0.52
Eanes	CSR4.0	0.32	0.90	0.40	1.08	0.65	1.55	0.98	0.51
Schrama-Ray	950308	0.29	0.96	0.45	1.04	0.70	1.55	0.99	0.48
This report	GOT99.2	0.28	0.89	0.37	1.02	0.65	1.47	0.94	0.43

Note: Bottom pressure stations adjusted for S_2 air tide via Haurwitz-Cowley model.

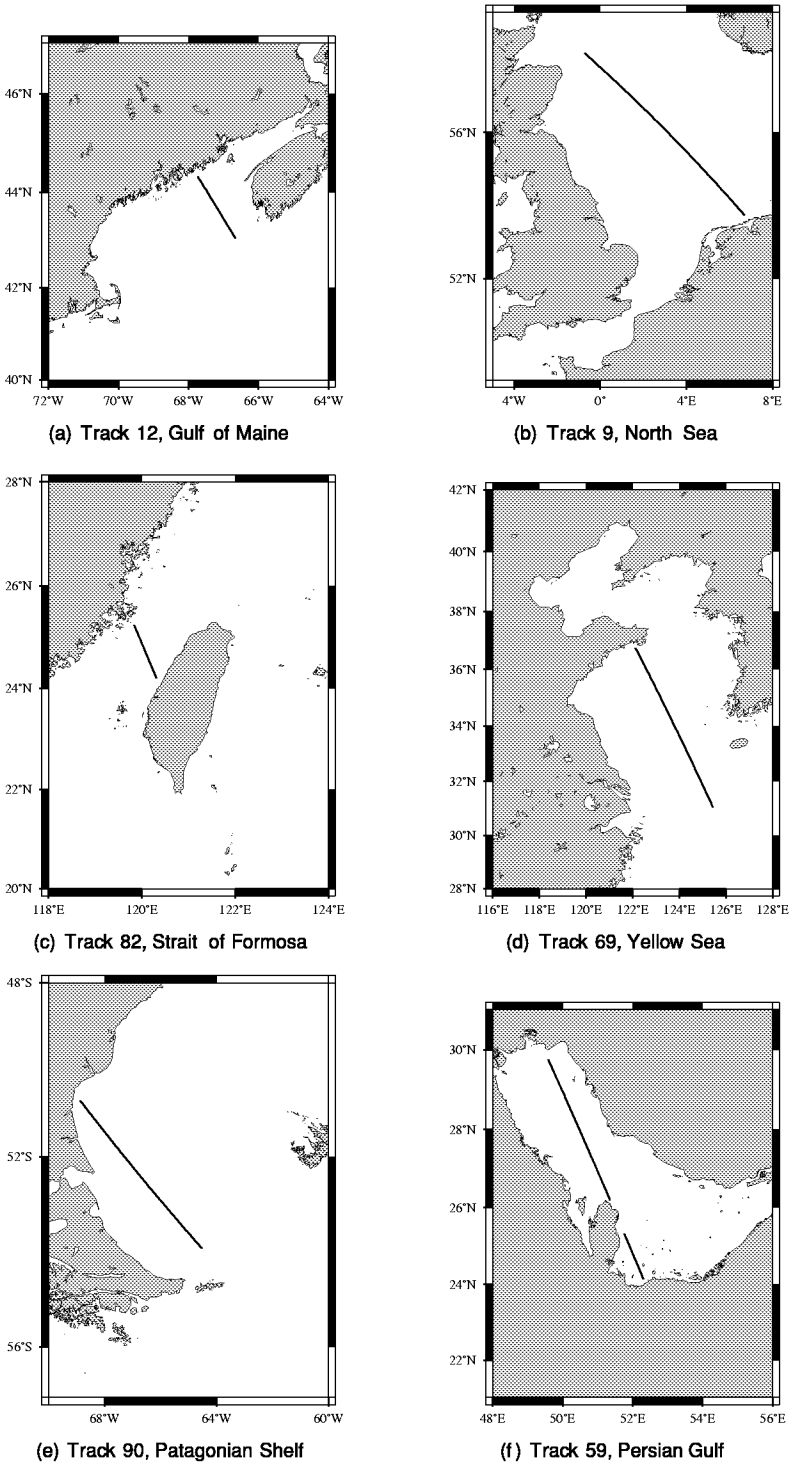

(a) Track 12, Gulf of Maine

(b) Track 9, North Sea

(c) Track 82, Strait of Formosa

(d) Track 69, Yellow Sea

(e) Track 90, Patagonian Shelf

(f) Track 59, Persian Gulf

Figure 2: TOPEX/POSEIDON tracks used in variance reduction tests.

Table 3: RMS (cm) of corrected sea level along partial track 12

index	latitude	longitude	ncycles	no correction	GOT99.2	CSR4.0
2442	44.321	292.268	100	123.29	13.26	65.53
2443	44.277	292.306	149	122.85	13.01	65.32
2444	44.233	292.344	167	121.58	13.32	65.65
2445	44.189	292.382	201	120.64	12.49	65.86
2446	44.145	292.419	210	119.96	11.93	66.56
2447	44.101	292.457	211	120.15	11.83	67.23
2448	44.057	292.495	214	119.94	11.83	67.73
2449	44.013	292.532	215	119.43	11.30	68.11
2450	43.969	292.570	217	118.69	11.94	67.87
2451	43.925	292.607	213	116.47	11.89	65.54
2452	43.881	292.644	211	114.69	11.72	62.27
2453	43.836	292.682	213	114.33	11.28	58.94
2454	43.792	292.719	219	113.67	11.15	54.25
2455	43.748	292.756	220	111.95	11.60	48.05
2456	43.704	292.793	217	110.19	11.58	40.96
2457	43.660	292.830	218	108.38	11.14	32.03
2458	43.615	292.867	215	106.07	10.71	22.63
2459	43.571	292.904	217	103.70	11.12	14.20
2460	43.527	292.941	217	102.92	11.72	12.31
2461	43.483	292.978	216	100.52	11.53	18.38
2462	43.438	293.015	215	98.35	11.10	20.96
2463	43.394	293.051	213	97.34	12.27	21.01
2464	43.350	293.088	215	94.82	11.73	21.20
2465	43.305	293.124	215	93.84	11.46	20.56
2466	43.261	293.161	214	91.54	13.21	22.38
2467	43.217	293.197	212	87.52	10.21	21.78
2468	43.172	293.234	211	84.02	9.62	23.00
2469	43.128	293.270	210	81.44	10.48	23.96
2470	43.083	293.306	216	78.54	9.10	25.06
2471	43.039	293.343	217	77.05	8.81	26.28

ing, 1998].) However, a few tests have been done on some selected T/P tracks in relatively shallow waters or in enclosed seas such as the Persian Gulf (where the present model benefits from the prior model of *Proctor et al.* [1994]). Six such cases are examined. All involve short track segments of T/P collinear data. Along these tracks, corrections from different tide models are applied and the variance of the resulting altimetric sea level variations at each point calculated. (The seasonal variation in sea level, which could be large in some locations, is *not* removed.) Two models (of the ocean + load tide) are used in these tests: the present GOT99.2 and the CSR4.0. The six tracks are shown in Figure 2. (The track numbering scheme follows the original Pathfinder data [*Koblinsky et al.*, 1999].)

Table 3 gives the detailed comparison at each of 30 1-sec locations along track 12 in the Gulf of Maine. At each location the tabulated entries include the number of T/P repeat cycles containing valid data and the rms of observed sea level

Table 4: Mean RMS (cm) of corrected sea level

Area	Track	No. pts.	No correction	GOT99.2	CSR4.0
Gulf of Maine	12	30	106.1	11.5	45.9
Persian Gulf	59	102	40.7	14.0	24.1
Yellow Sea	69	123	59.3	15.1	15.5
Patagonian Shelf	90	82	180.0	15.8	17.3
Formosa Strait	82	23	144.4	25.1	34.0
North Sea	9	116	39.7	18.5	18.7

over those cycles when (a) no tide correction is applied, (b) the CSR4.0 correction is applied, and (c) the present GOT99.2 correction is applied. Along this particular track both models reduce the sea level variance, but clearly the CSR4.0 model leaves a large residual tide. Of course, the present solution benefits from having a reasonably accurate prior model in this region.

Table 4 shows the mean rms of uncorrected and corrected sea level for all six test tracks. As is evident from Track 12, some individual locations can have variances considerably larger than the tabulated means. While one may expect that both models may be inadequate in some of these near-coastal regions and that local tide models could perhaps do better, the present model appears to represent an advance as far as global models are concerned.

5 Spherical Harmonic Coefficients

This section tabulates some of the low-degree spherical harmonic coefficients of the GOT99.2 TOPEX/POSEIDON ocean tide solution. Because the data are available on very nearly a global grid, with only a few small inlets and bays missing, the spherical harmonic coefficients may be determined by straightforward numerical integration. And since the grid is of resolution 0.5°, the harmonic coefficients can be easily computed at least through degree and order 360. For practical reasons only a few low-degree coefficients are tabulated in this report. More complete sets are available from the author.

The degree-1 and degree-2 coefficients are especially important to a wide range of geodetic and geophysical applications. For example, the degree-1 coefficients completely describe the tidal oscillations of the geocenter position which can be compared with observations from satellite laser ranging. The degree-2 coefficients describe tidal variations in the Earth's inertia tensor and the tidal braking torques. The coefficients are tabulated complete through degree and order 4. Some additional coefficients that induce long-period perturbations in satellite orbits (order 1 diurnals and order 2 semidiurnals) are also tabulated through degree 10; these are useful for comparisons to satellite laser ranging analyses. The coefficients describe the usual bottom-relative tide; i.e., the load tide has been removed.

There are as many conventions used for spherical harmonic components of

Table 5: Normalized Associated Legendre Functions.

$$\bar{P}_0^0(x) = \sqrt{(1/2)}$$
$$\bar{P}_1^0(x) = \sqrt{(3/2)}\, x$$
$$\bar{P}_1^1(x) = \sqrt{(3/4)}\, (1-x^2)^{1/2}$$
$$\bar{P}_2^0(x) = \sqrt{(5/2)}\, (\tfrac{3}{2}x^2 - \tfrac{1}{2})$$
$$\bar{P}_2^1(x) = \sqrt{(5/12)}\, 3x(1-x^2)^{1/2}$$
$$\bar{P}_2^2(x) = \sqrt{(5/48)}\, 3(1-x^2)$$
$$\bar{P}_3^0(x) = \sqrt{(7/2)}\, (\tfrac{5}{2}x^3 - \tfrac{3}{2}x)$$
$$\bar{P}_3^1(x) = \sqrt{(7/24)}\, (\tfrac{15}{2}x^2 - \tfrac{3}{2})(1-x^2)^{1/2}$$
$$\bar{P}_3^2(x) = \sqrt{(7/240)}\, 15x(1-x^2)$$
$$\bar{P}_3^3(x) = \sqrt{(7/1440)}\, 15(1-x^2)^{3/2}$$

tides as there are authors.[2] Two conventions are used here in the hope that readers might find one or the other more useful. The first follows conventions used in some of our earlier work in which any spherical harmonic series is expressed in the following convention:

$$\tfrac{1}{2}\sum_{n=0}^{N} a_{n0}\bar{P}_n^0(\cos\theta) + \sum_{n=1}^{N}\sum_{m=1}^{n}(a_{nm}\cos m\phi - b_{nm}\sin m\phi)\bar{P}_n^m(\cos\theta). \qquad (1)$$

The $\bar{P}_n^m(\mu)$ are the normalized associated Legendre functions, the first few of which are given in Table 5. For any particular tidal constituent the elevation is given by

$$\zeta(\theta,\phi,t) = H(\theta,\phi)\ \cos(\omega t - G(\theta,\phi)$$

for amplitude H and Greenwich phase lag G. The in-phase and quadrature components $H\cos G$ and $H\sin G$ are then expanded as follows:

$$H\cos G = \sum_{n=0}^{N}\sum_{m=0}^{n}{}'(a_{nm}\cos m\phi - b_{nm}\sin m\phi)\bar{P}_n^m(\cos\theta)$$

$$H\sin G = \sum_{n=0}^{N}\sum_{m=0}^{n}{}'(c_{nm}\cos m\phi - d_{nm}\sin m\phi)\bar{P}_n^m(\cos\theta)$$

where the prime on the second summation indicates that the first term is multiplied by $\frac{1}{2}$, in agreement with (1). The coefficients a_{nm}, b_{nm}, c_{nm}, and d_{nm} are listed in the following tables in units of millimeters.

The second convention in these tables follows more closely one used in satellite geodesy (except for various phase variations). Here the tide is expressed as a series of prograde and retrograde waves with amplitudes D_{nm}^{+} and D_{nm}^{-} and phase lags

[2]More, actually. Because some authors (myself included) have employed inconsistent conventions from one paper to the next.

ψ^+_{nm} and ψ^-_{nm}, respectively. (Some authors prefer phase *leads* $\varepsilon^\pm_{nm}$ with possibly additional increments of $\pm 90°$.) The tidal constituent ζ is then expressed as[3]

$$\zeta(\theta,\phi,t) = \sum_{n,m} \left\{ D^+_{nm} \cos(\omega t + m\phi - \psi^+_{nm}) + D^-_{nm} \cos(\omega t - m\phi - \psi^-_{nm}) \right\} P^m_n(\cos\theta), \tag{2}$$

where here $P^m_n(\cos\theta)$ is unnormalized. The following formulae convert between the two conventions:

$$D^\pm_{nm} \cos\psi^\pm_{nm} = \tfrac{1}{2}(a_{nm} \pm d_{nm}) N^m_n$$

$$D^\pm_{nm} \sin\psi^\pm_{nm} = \tfrac{1}{2}(c_{nm} \mp b_{nm}) N^m_n$$

where the normalization factor N^m_n is given by

$$N^m_n = \left[\frac{2n+1}{2} \frac{(n-m)!}{(n+m)!} \right]^{1/2}.$$

In both adopted conventions the argument ωt implicitly represents the full Doodson argument (for a cosine function; hence the argument includes the necessary $-90°$ to account for Doodson's original use of the sine function for diurnal tides [similar to Cartwright-Tayler] and a possible $+180°$ to ensure positive constituent amplitudes in the generating potential). For example, for K_1 $\omega t = 15°T + h + 90°$ where T is mean Greenwich time and h is the mean longitude of the sun. See *Doodson and Warburg* (1941).

Tables 6–13 give the spherical harmonic coefficients for the eight short-period tides in order of frequency. The units are millimeters (except for $\psi^\pm_{nm}$ in degrees).

[3]This convention is consistent with CR91 and SR94 except for the phase lags $\psi^\pm_{nm}$ of the diurnal tides which are offset by 90°. In the present convention, for example, work and torque integrals are proportional to $D^+_{2,m} \sin\psi^+_{2,m}$ for all tides, whereas in CR91 they were proportional to $D^+_{2,1} \cos\psi^+_{2,1}$ for diurnal tides and $D^+_{2,2} \sin\psi^+_{2,2}$ for semidiurnal tides.

Table 6: Spherical harmonic coefficients for Q_1.

n	m	$a_{n,m}$	$b_{n,m}$	$c_{n,m}$	$d_{n,m}$	$D^+_{n,m}$	$\psi^+_{n,m}$	$D^-_{n,m}$	$\psi^-_{n,m}$
1	0	1.18		-4.84		3.05	283.72		
1	1	1.31	-1.30	.12	-.38	.74	56.92	.89	325.10
2	0	2.96		-3.09		3.38	313.82		
2	1	-5.41	-10.48	1.80	-7.58	5.77	136.62	2.89	284.04
2	2	2.59	-.17	-1.84	3.23	.98	344.01	.34	252.46
3	0	1.31		.36		1.27	15.53		
3	1	5.94	6.51	2.12	7.24	3.75	341.58	2.36	98.53
3	2	1.38	5.01	-2.67	1.32	.69	289.31	.20	88.53
3	3	-8.25	-7.66	2.51	.74	.44	126.46	.36	209.79
4	0	.33		6.68		7.09	87.20		
4	1	-7.07	.25	4.29	-5.86	3.21	162.63	1.12	104.99
4	2	1.41	3.76	-2.89	.98	.40	289.76	.05	63.32
4	3	-.04	-2.52	2.29	-7.01	.13	145.66	.10	358.11
4	4	1.27	5.61	-.41	-.36	.03	278.60	.03	72.60
5	1	6.08	.49	-3.74	3.81	2.30	336.87	.85	304.89
6	1	-1.81	-.83	-.21	-1.62	.69	169.80	.21	259.83
7	1	2.24	.26	-2.41	.58	.71	316.50	.50	307.69
8	1	-.05	.95	.52	.62	.12	322.60	.28	114.33
9	1	1.05	-.90	.30	-.51	.21	65.76	.27	338.93
10	1	.92	-.06	-.27	1.24	.33	354.20	.07	225.62

Table 7: Spherical harmonic coefficients for O_1.

n	m	$a_{n,m}$	$b_{n,m}$	$c_{n,m}$	$d_{n,m}$	$D^+_{n,m}$	$\psi^+_{n,m}$	$D^-_{n,m}$	$\psi^-_{n,m}$
1	0	3.03		-24.97		15.40	276.91		
1	1	7.62	-5.53	1.36	-4.24	3.32	63.87	5.44	340.63
2	0	10.64		-5.97		9.65	330.70		
2	1	-19.66	-43.54	12.10	-38.04	25.87	136.04	11.75	300.32
2	2	15.99	4.34	-8.04	17.57	5.77	339.75	.65	246.89
3	0	7.02		7.14		9.37	45.49		
3	1	16.13	17.01	23.06	35.23	13.97	6.71	11.99	115.49
3	2	10.99	26.42	-8.17	18.69	3.89	310.63	1.69	112.88
3	3	-36.98	-41.44	4.56	-11.33	2.33	136.41	1.57	235.19
4	0	-3.97		20.39		22.03	101.02		
4	1	-39.32	5.97	15.69	-25.73	15.60	171.50	6.06	122.10
4	2	6.53	13.05	-12.78	8.91	1.68	300.88	.13	173.45
4	3	-4.22	-4.55	16.12	-29.88	.60	148.79	.42	24.27
4	4	9.74	30.65	.78	2.09	.17	291.60	.17	76.33
5	1	26.28	2.17	-15.80	17.93	10.22	337.87	3.42	301.51
6	1	-7.71	-4.88	-2.19	-5.06	2.57	168.13	1.49	249.42
7	1	10.48	2.44	-11.52	.80	3.28	308.96	2.43	316.84
8	1	2.16	3.45	2.25	4.81	1.21	350.24	1.08	114.96
9	1	4.76	-1.02	.51	-3.79	.29	57.57	1.39	356.57
10	1	6.36	.77	.48	5.60	1.85	358.61	.23	59.18

Table 8: Spherical harmonic coefficients for P_1.

n	m	$a_{n,m}$	$b_{n,m}$	$c_{n,m}$	$d_{n,m}$	$D^+_{n,m}$	$\psi^+_{n,m}$	$D^-_{n,m}$	$\psi^-_{n,m}$
1	0	3.40		-13.02		8.24	284.65		
1	1	3.93	-1.77	2.11	-3.57	1.69	84.63	3.25	2.61
2	0	-1.89		-1.56		1.94	219.56		
2	1	-4.87	-16.89	5.97	-15.57	9.90	131.79	4.94	314.41
2	2	8.76	1.26	-1.24	11.83	3.35	353.07	.50	179.51
3	0	6.16		5.45		7.69	41.53		
3	1	-3.16	2.60	12.30	11.62	3.48	48.89	5.67	134.79
3	2	1.70	8.13	1.00	16.12	1.64	338.18	1.46	147.65
3	3	-15.70	-17.59	-2.34	-14.15	1.17	152.94	.70	265.56
4	0	1.71		5.87		6.49	73.73		
4	1	-18.21	7.83	.81	-10.31	6.97	193.83	2.78	132.40
4	2	3.65	3.68	-7.04	2.49	.69	299.83	.20	289.08
4	3	-4.81	.60	6.18	-10.67	.25	160.19	.13	49.14
4	4	4.89	17.76	5.36	5.35	.08	309.55	.12	91.12
5	1	12.46	-1.76	-7.21	8.53	4.64	345.44	2.10	293.68
6	1	-3.48	-2.55	-3.11	-1.14	.92	186.85	1.20	247.60
7	1	5.79	1.00	-4.60	1.14	1.63	321.06	1.08	322.15
8	1	.26	.93	-.03	1.05	.28	323.67	.21	131.19
9	1	2.87	-.03	.87	-.16	.46	18.31	.51	15.45
10	1	1.32	-.34	1.07	3.26	.74	17.09	.32	159.28

Table 9: Spherical harmonic coefficients for K_1.

n	m	$a_{n,m}$	$b_{n,m}$	$c_{n,m}$	$d_{n,m}$	$D^+_{n,m}$	$\psi^+_{n,m}$	$D^-_{n,m}$	$\psi^-_{n,m}$
1	0	10.77		-39.69		25.18	285.19		
1	1	11.97	-5.16	6.75	-11.16	5.17	86.12	10.04	3.92
2	0	-7.39		-4.43		6.81	210.94		
2	1	-13.66	-50.24	18.12	-46.53	29.40	131.36	14.83	315.66
2	2	26.80	3.64	-3.13	36.65	10.30	353.91	1.59	177.06
3	0	19.31		16.99		24.06	41.35		
3	1	-12.15	6.55	37.55	33.97	10.24	54.86	17.23	136.28
3	2	4.31	23.56	4.19	50.53	4.97	340.54	4.60	149.02
3	3	-47.08	-52.75	-8.16	-44.93	3.56	154.15	2.12	267.98
4	0	6.05		16.87		19.01	70.27		
4	1	-55.01	24.91	.88	-30.76	21.13	195.65	8.40	133.24
4	2	11.19	10.53	-21.54	7.12	2.06	299.73	.66	290.27
4	3	-15.23	2.47	18.35	-31.47	.74	161.22	.39	52.05
4	4	14.87	54.52	17.42	17.22	.26	310.87	.38	91.87
5	1	37.70	-5.98	-21.75	25.81	14.01	346.06	6.46	293.21
6	1	-10.48	-7.78	-9.90	-3.16	2.72	188.83	3.76	247.52
7	1	17.71	2.97	-13.73	3.64	4.96	321.97	3.24	322.61
8	1	.59	2.65	-.34	2.88	.79	319.18	.56	134.71
9	1	8.83	.02	2.77	-.09	1.49	17.50	1.52	17.38
10	1	3.60	-1.19	3.44	10.01	2.22	18.80	1.05	160.67

Table 10: Spherical harmonic coefficients for N_2.

n	m	$a_{n,m}$	$b_{n,m}$	$c_{n,m}$	$d_{n,m}$	$D^+_{n,m}$	$\psi^+_{n,m}$	$D^-_{n,m}$	$\psi^-_{n,m}$
1	0	3.10		2.05		2.27	33.47		
1	1	1.05	1.49	-1.44	-.47	1.29	281.35	.66	2.14
2	0	-.59		-2.77		2.24	257.91		
2	1	-5.88	-1.21	1.31	-1.56	2.53	161.34	1.39	178.69
2	2	-7.51	-17.98	19.30	-14.40	6.98	120.43	1.13	10.86
3	0	5.39		-12.91		13.08	292.65		
3	1	8.71	3.65	11.66	-9.45	2.17	95.29	6.42	40.12
3	2	.57	7.57	-4.17	1.96	1.03	282.14	.31	112.29
3	3	26.12	-9.17	6.91	-1.71	1.02	33.39	.97	355.36
4	0	-13.57		4.26		15.09	162.58		
4	1	7.91	1.90	11.35	4.20	3.64	37.95	3.26	74.36
4	2	20.20	25.82	-6.84	6.53	2.36	309.30	1.31	54.22
4	3	-17.89	19.19	-4.11	10.54	.36	252.50	.48	152.05
4	4	-21.06	-10.73	10.82	-4.95	.18	140.36	.09	179.67
5	2	-19.26	-6.24	12.76	21.02	.77	84.70	1.65	170.81
6	2	1.71	-15.71	5.53	-2.87	.66	93.14	.35	294.19
7	2	3.99	-4.85	-10.13	-12.56	.25	211.65	.56	317.82
8	2	-3.32	2.32	-6.43	-4.27	.24	229.03	.09	282.96
9	2	.71	4.48	2.05	-.97	.04	263.84	.12	75.59
10	2	2.17	-3.02	.16	-1.94	.05	85.83	.07	325.11

Table 11: Spherical harmonic coefficients for M_2.

n	m	$a_{n,m}$	$b_{n,m}$	$c_{n,m}$	$d_{n,m}$	$D^+_{n,m}$	$\psi^+_{n,m}$	$D^-_{n,m}$	$\psi^-_{n,m}$
1	0	10.74		13.82		10.72	52.15		
1	1	8.58	6.99	-5.61	1.47	6.98	308.56	3.13	10.98
2	0	-2.60		-36.27		28.75	265.91		
2	1	-24.93	10.26	-5.37	-14.49	13.69	201.63	3.72	154.93
2	2	-47.66	-67.52	85.87	-80.91	32.30	129.97	6.13	28.90
3	0	19.44		-36.44		38.63	298.08		
3	1	31.04	23.47	73.97	-42.86	14.01	103.17	33.02	52.82
3	2	-6.63	25.28	-8.51	12.82	2.93	280.39	2.19	139.24
3	3	102.24	-42.50	62.76	-26.85	4.51	54.38	4.56	8.92
4	0	-44.13		20.41		51.57	155.18		
4	1	12.69	-6.33	74.81	34.61	22.27	59.76	17.05	107.75
4	2	72.83	96.72	-22.56	72.41	10.51	320.60	4.15	89.68
4	3	-73.86	87.28	-62.56	76.49	2.24	271.00	2.28	170.66
4	4	-93.78	-67.31	11.90	-34.05	.79	148.21	.43	222.85
5	2	-79.46	-54.10	15.24	89.95	2.84	81.40	7.03	192.92
6	2	-16.47	-68.06	46.15	-47.25	4.07	119.16	1.18	324.56
7	2	33.03	3.13	-40.74	-53.94	1.21	244.52	2.36	336.61
8	2	-10.35	13.61	-41.60	-23.89	1.33	238.19	.64	295.81
9	2	7.30	24.78	10.87	7.71	.35	317.18	.62	90.66
10	2	9.84	-7.80	6.61	-15.34	.23	110.90	.37	357.31

Table 12: Spherical harmonic coefficients for S_2.

n	m	$a_{n,m}$	$b_{n,m}$	$c_{n,m}$	$d_{n,m}$	$D^+_{n,m}$	$\psi^+_{n,m}$	$D^-_{n,m}$	$\psi^-_{n,m}$
1	0	2.22		5.99		3.91	69.62		
1	1	3.67	.86	1.62	2.32	2.61	7.21	1.23	61.34
2	0	10.09		-10.86		11.72	312.88		
2	1	-4.31	13.54	-3.65	1.67	5.61	261.28	3.73	121.19
2	2	-22.60	-19.73	36.71	-24.95	11.91	130.12	2.77	82.13
3	0	9.61		-18.66		19.63	297.25		
3	1	-11.10	12.38	26.73	-1.57	5.17	131.43	10.87	103.69
3	2	-9.26	10.31	-22.21	-4.74	3.02	246.70	1.09	249.22
3	3	12.61	6.89	24.84	-26.40	.79	127.53	1.75	39.12
4	0	-27.10		4.15		29.08	171.30		
4	1	-7.45	-13.87	32.95	-5.00	11.49	104.88	4.56	97.31
4	2	35.70	11.48	-6.58	27.05	3.65	343.94	.56	29.50
4	3	8.18	7.72	-19.64	49.78	.96	334.74	.65	195.99
4	4	-22.69	-29.33	-4.34	-32.56	.32	155.66	.19	286.33
5	2	-18.95	-27.04	7.32	31.87	1.49	69.39	2.21	201.21
6	2	-24.57	-12.26	3.06	-30.79	1.79	164.53	.35	304.08
7	2	15.95	10.93	-5.59	-9.68	.44	290.82	.65	11.77
8	2	6.96	9.05	-13.57	-11.07	.47	259.69	.38	345.93
9	2	3.89	1.99	8.60	9.45	.26	26.37	.21	117.74
10	2	-2.19	.89	9.25	-7.18	.19	138.26	.17	63.79

Table 13: Spherical harmonic coefficients for K_2.

n	m	$a_{n,m}$	$b_{n,m}$	$c_{n,m}$	$d_{n,m}$	$D^+_{n,m}$	$\psi^+_{n,m}$	$D^-_{n,m}$	$\psi^-_{n,m}$
1	0	.83		1.86		1.25	66.08		
1	1	.82	.08	-.45	.65	.68	340.24	.18	293.97
2	0	2.22		-3.77		3.46	300.54		
2	1	-1.37	4.27	-1.15	.00	1.81	255.83	1.10	113.76
2	2	-6.14	-4.60	9.37	-7.11	3.11	133.48	.79	78.44
3	0	.77		-5.76		5.44	277.65		
3	1	-2.16	2.95	7.94	-.17	1.49	114.98	2.99	100.38
3	2	-3.14	3.02	-6.10	-1.59	.88	242.59	.29	243.23
3	3	4.03	1.18	6.72	-7.63	.23	123.04	.49	34.11
4	0	-6.67		2.21		7.46	161.64		
4	1	-2.16	-4.24	9.64	-1.36	3.39	104.23	1.30	98.48
4	2	10.25	4.17	-2.87	6.78	1.03	337.54	.21	20.54
4	3	2.30	3.06	-4.79	13.63	.27	333.78	.17	188.66
4	4	-6.26	-9.58	-.14	-9.24	.10	148.64	.05	287.08
5	2	-5.76	-7.08	2.53	9.80	.42	67.20	.66	196.29
6	2	-6.00	-4.12	1.40	-8.37	.48	158.98	.11	311.10
7	2	3.78	2.88	-2.26	-2.97	.13	279.00	.17	5.24
8	2	1.14	2.51	-3.27	-3.28	.13	249.69	.09	350.18
9	2	1.27	.38	2.55	2.73	.08	28.46	.06	116.44
10	2	-.39	.11	2.45	-2.03	.05	135.87	.05	57.38

A Global Cotidal Charts

The following pages display global charts of amplitude (cm) and Greenwich phase lag (degrees) for the eight diurnal and semidiurnal tides Q_1, O_1, P_1, K_1, N_2, M_2, S_2, and K_2 (listed in order of frequency), constituting the present GOT99.2 altimeter tide solution. The phases correspond to those traditionally adopted in tidal investigations and are reckoned with respect to the equilibrium Doodson arguments at Greenwich. Although altimetry strictly measures a geocentric (solid + ocean) tide, the solid tide has been removed (using methods described in the main body of this report), so the following charts are of the usual ocean tide as measured, for example, by a tide gauge.

Empirical solutions such as these are obviously susceptible to measurement noise, and noise is evident in a few places, particularly in smaller tides like Q_1, less so in larger tides like M_2. In regions of very low amplitude the phases are essentially indeterminate, so any measurement noise can cause phase contour lines to appear to wander around aimlessly. Readers accustomed to seeing cotidal charts derived from numerical computer models (where the only noise source might be from possibly poor numerics) may find such noise curious, but the compensation is that these charts are more accurate than any available numerical model can produce.

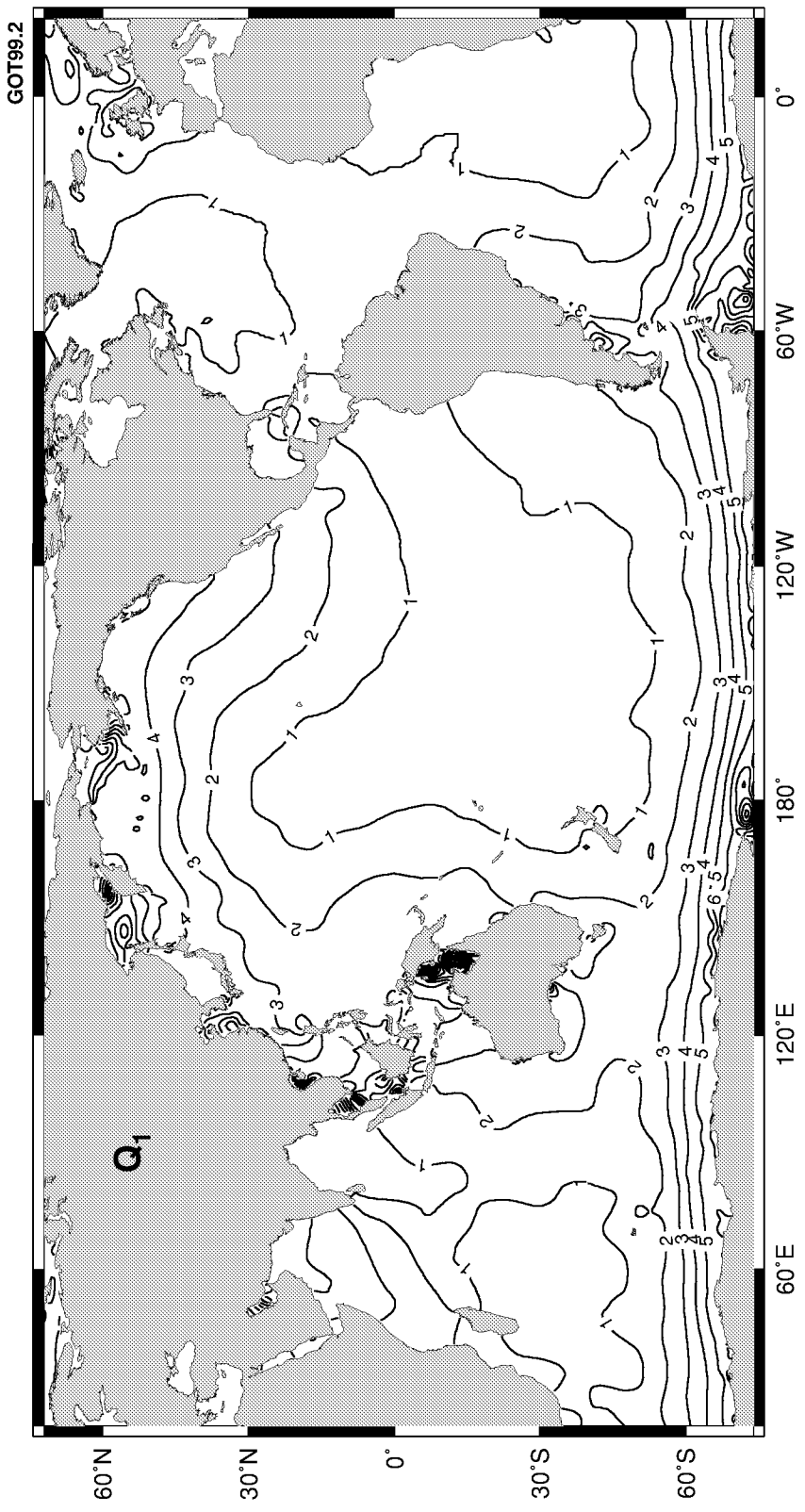

Figure A1. Amplitude of Q_1 tide. Contour interval = 1 cm.

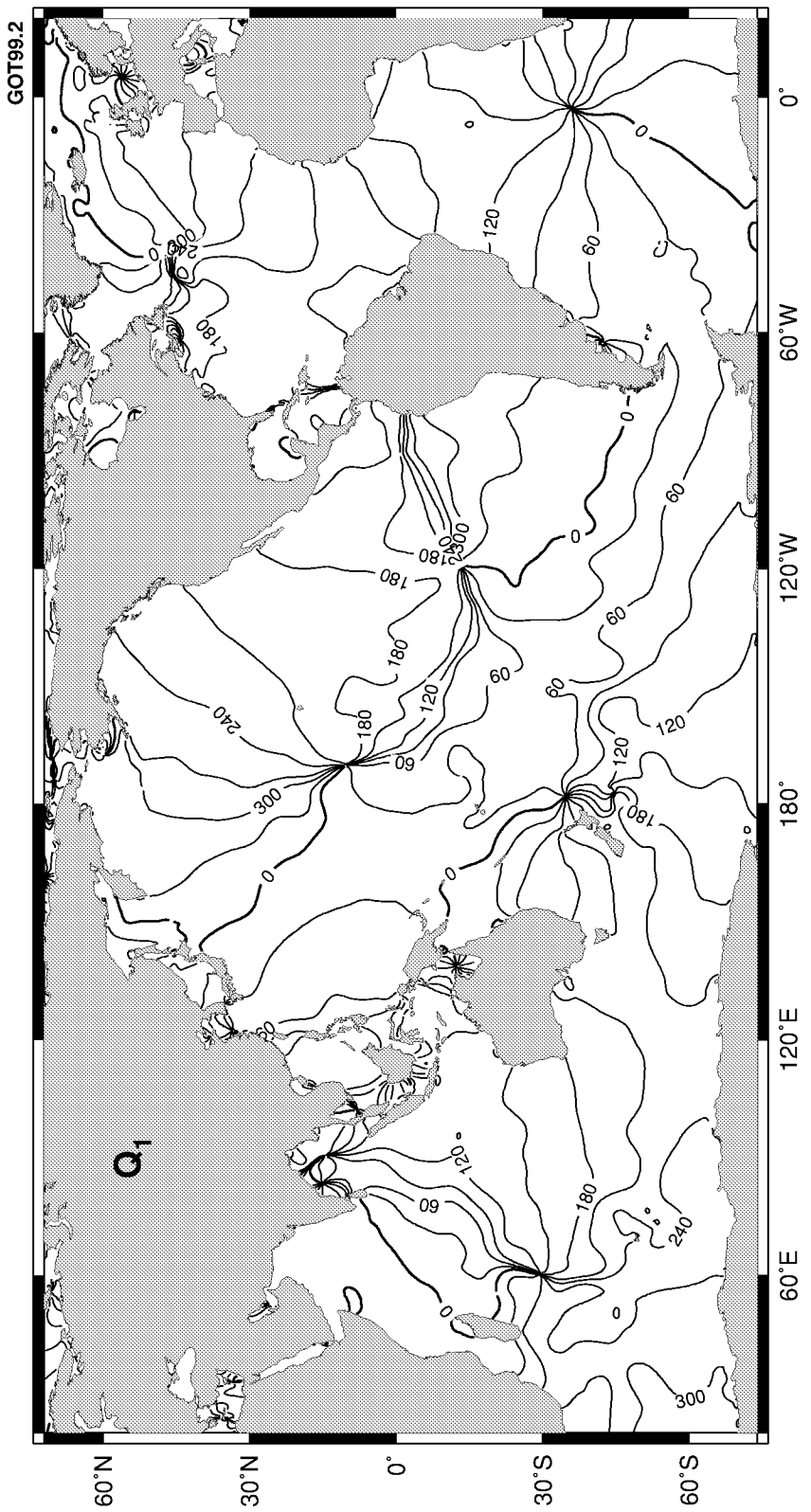

Figure A2. Greenwich phase lag of Q_1 tide. Contour interval = 30°.

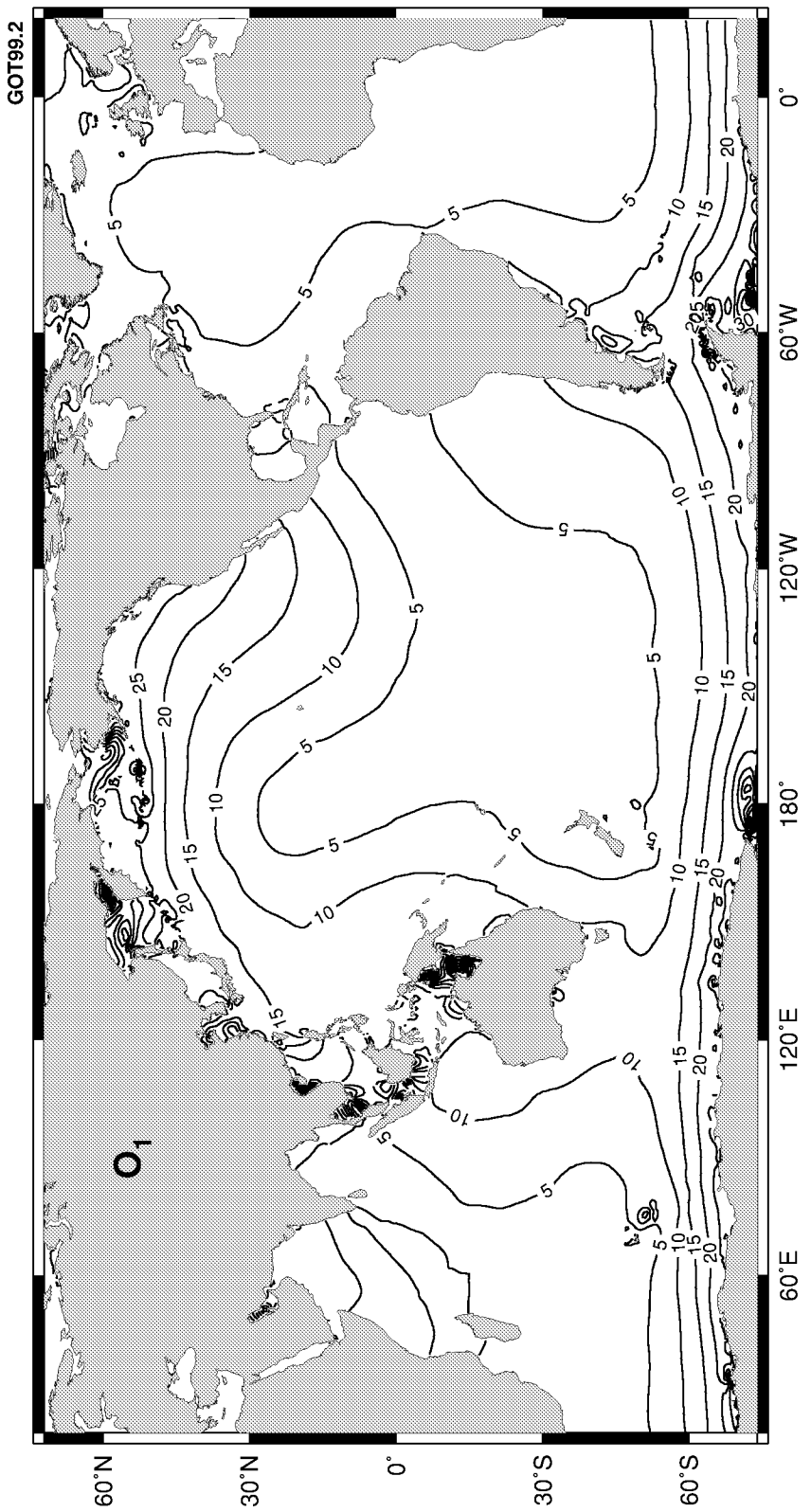

Figure A3. Amplitude of O_1 tide. Contour interval = 5 cm.

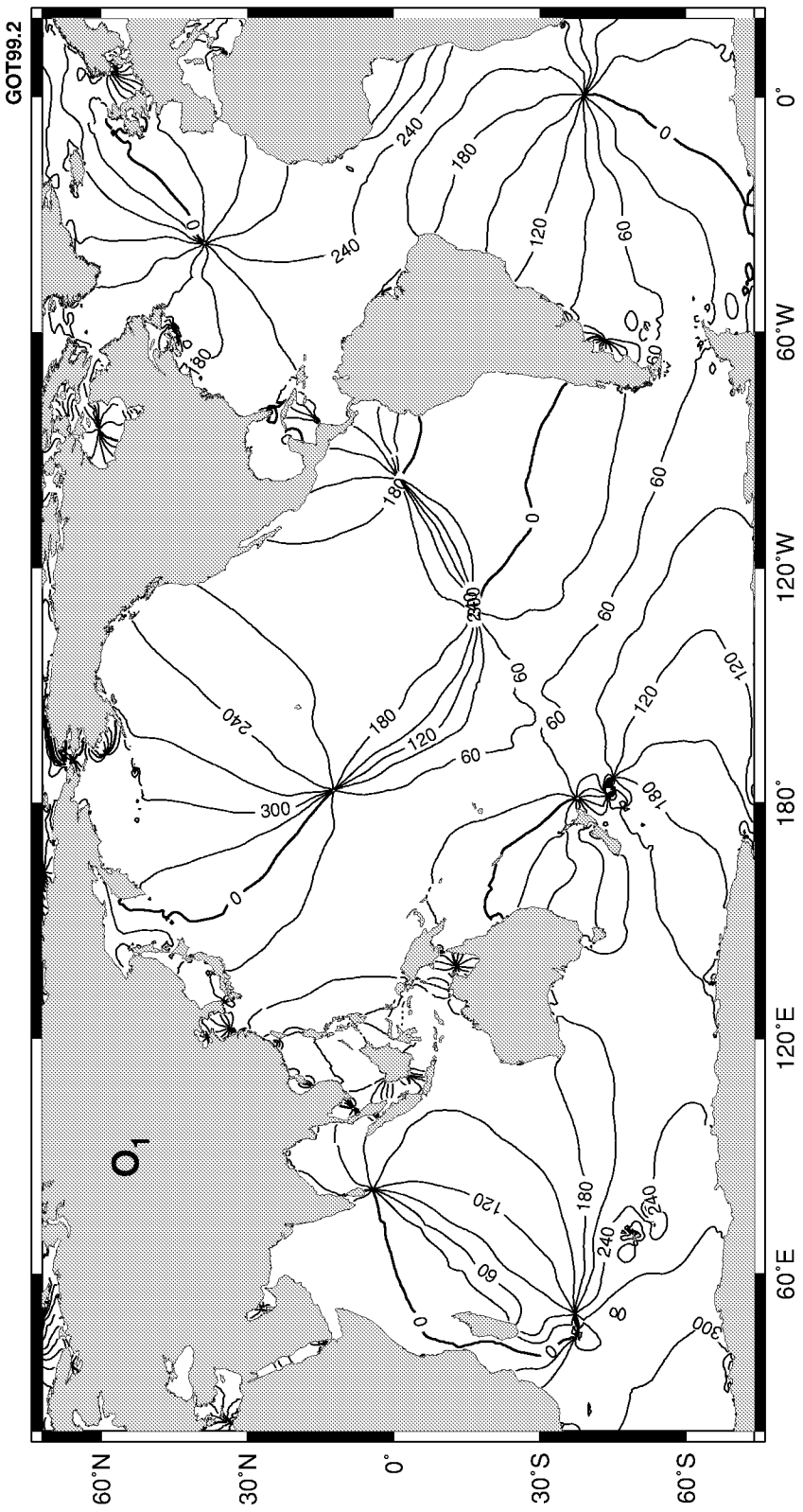

Figure A4. Greenwich phase lag of O_1 tide. Contour interval = 30°.

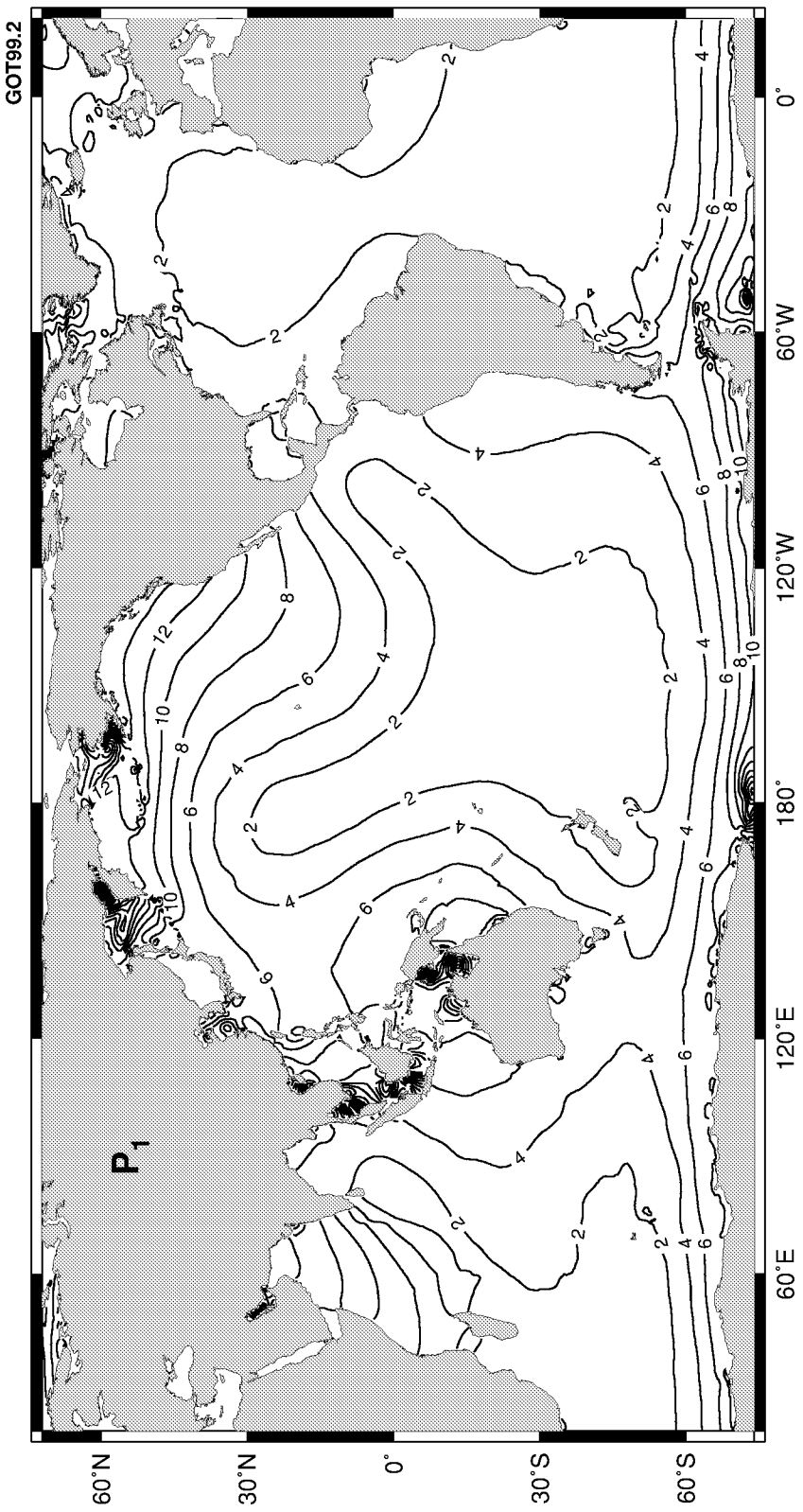

Figure A5. Amplitude of P_1 tide. Contour interval = 2 cm.

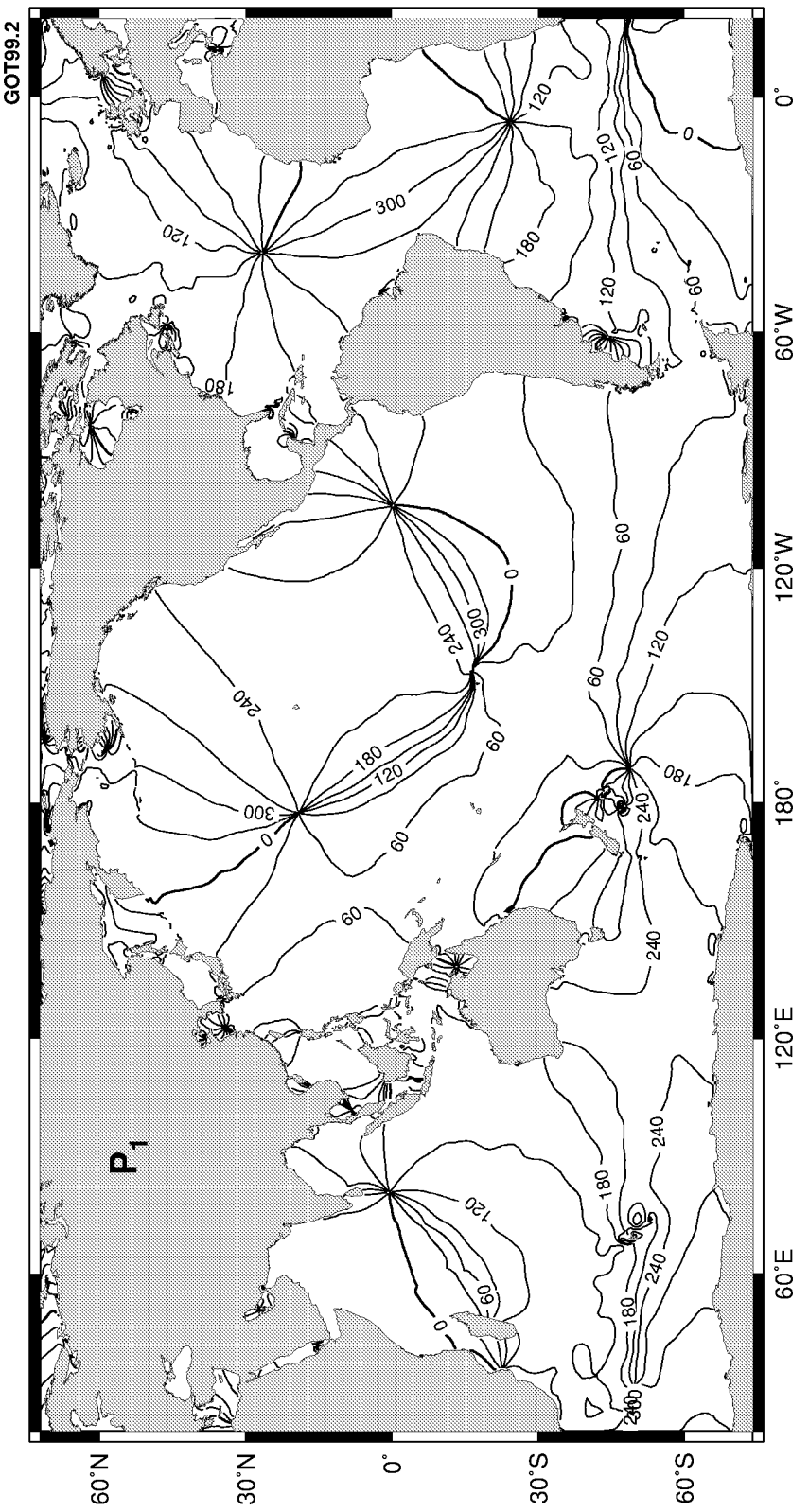

Figure A6. Greenwich phase lag of P_1 tide. Contour interval = 30°.

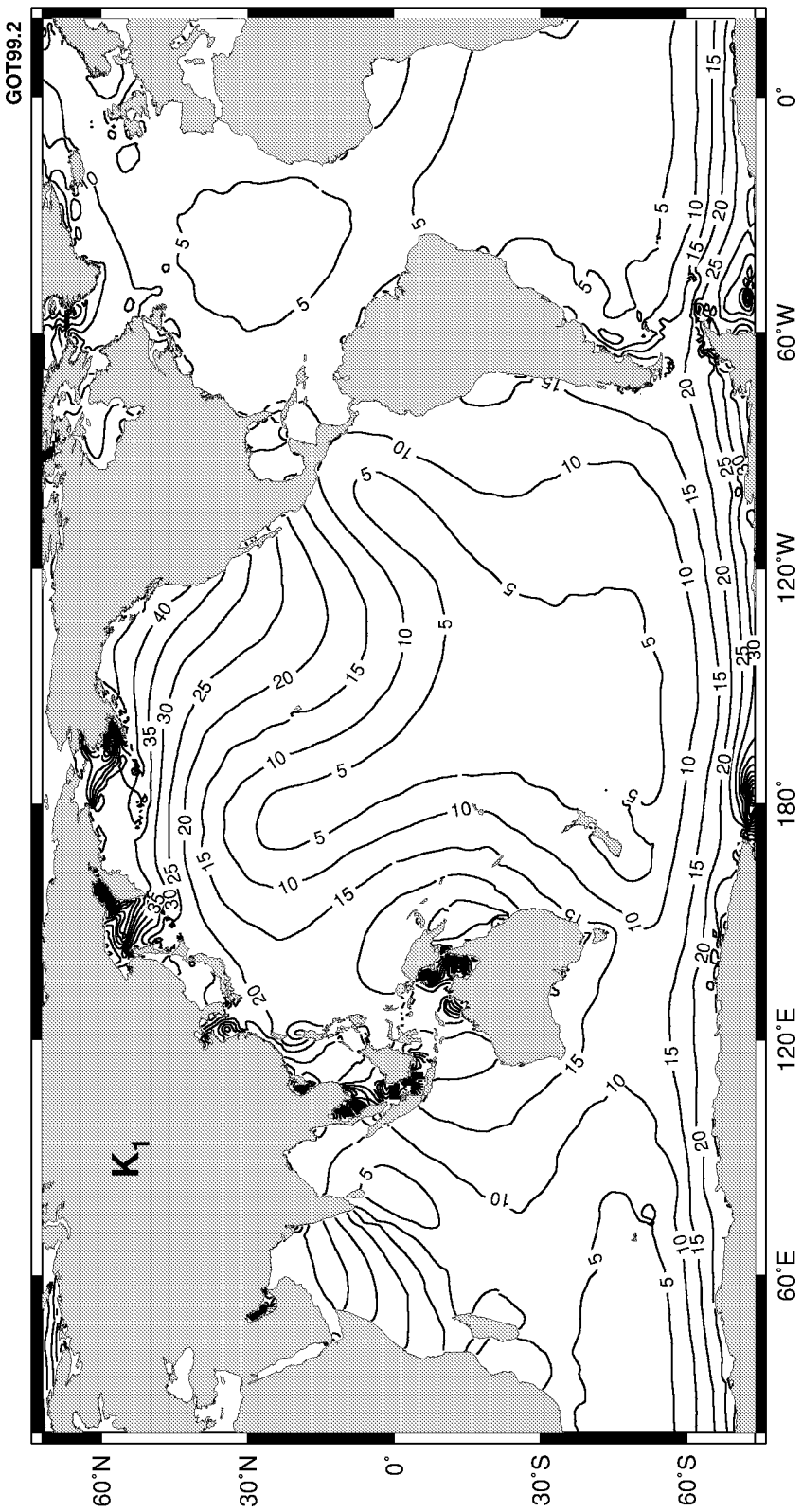

Figure A7. Amplitude of K_1 tide. Contour interval = 5 cm.

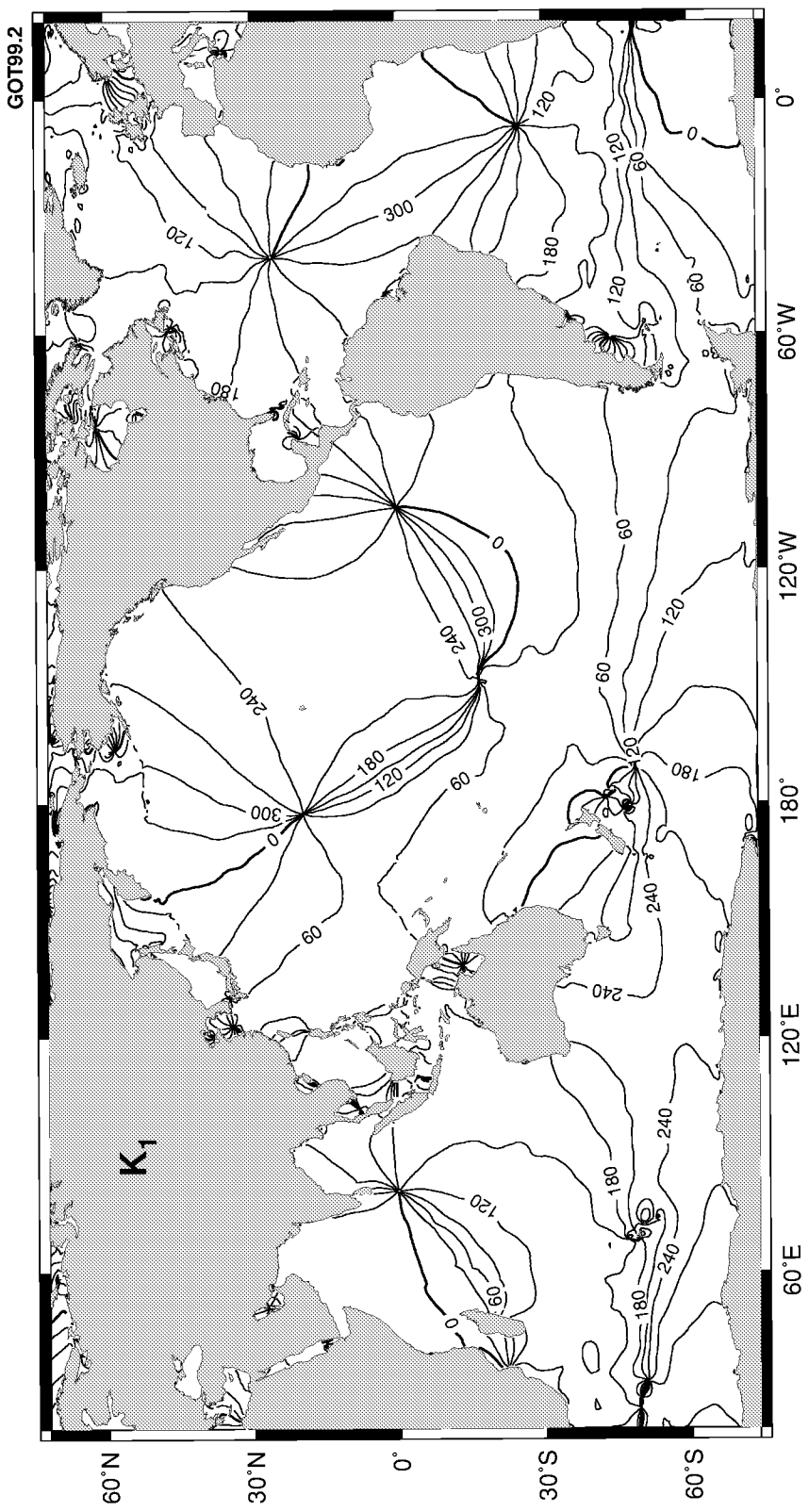

Figure A8. Greenwich phase lag of K_1 tide. Contour interval = 30°.

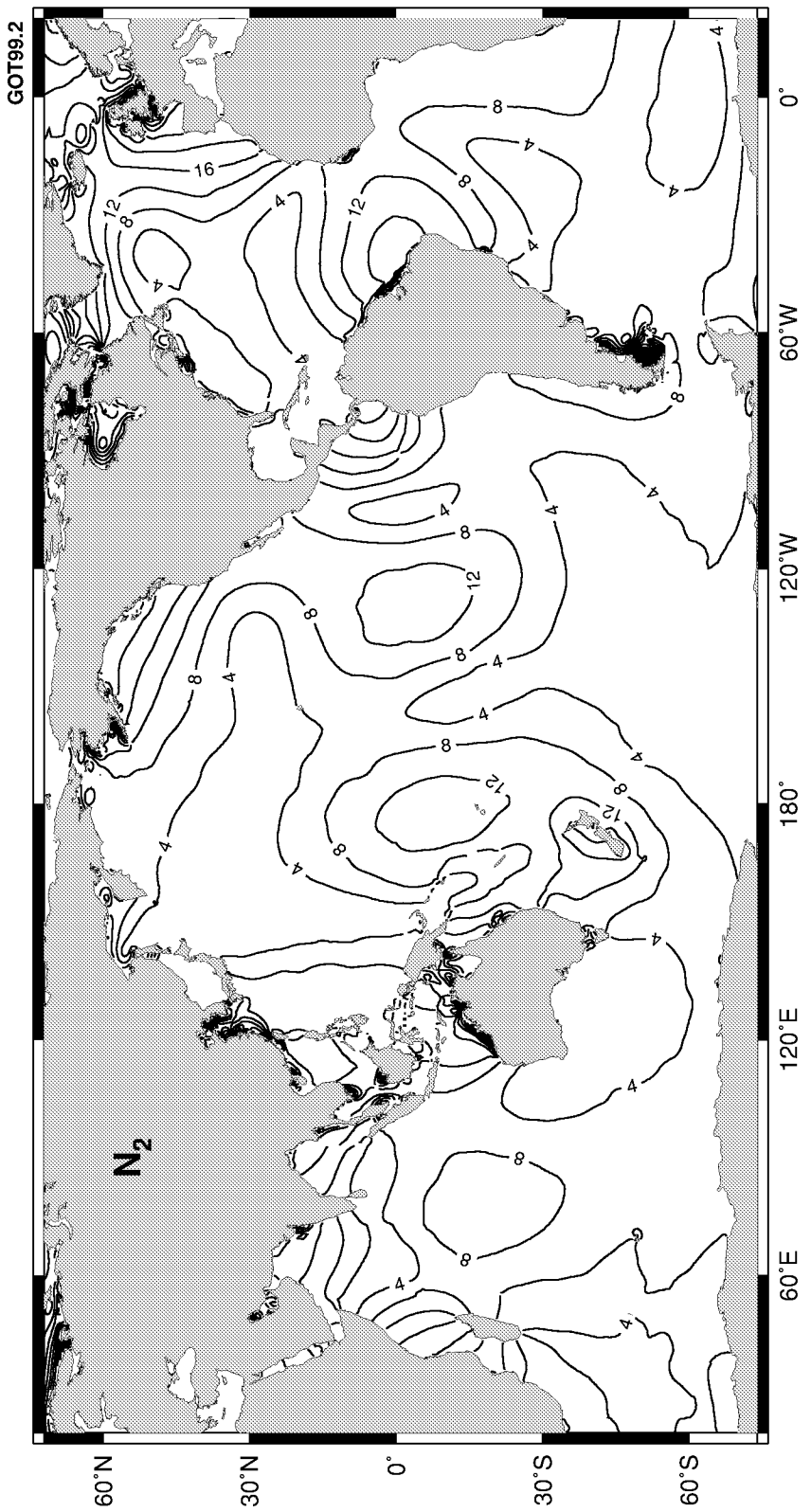

Figure A9. Amplitude of N_2 tide. Contour interval = 4 cm.

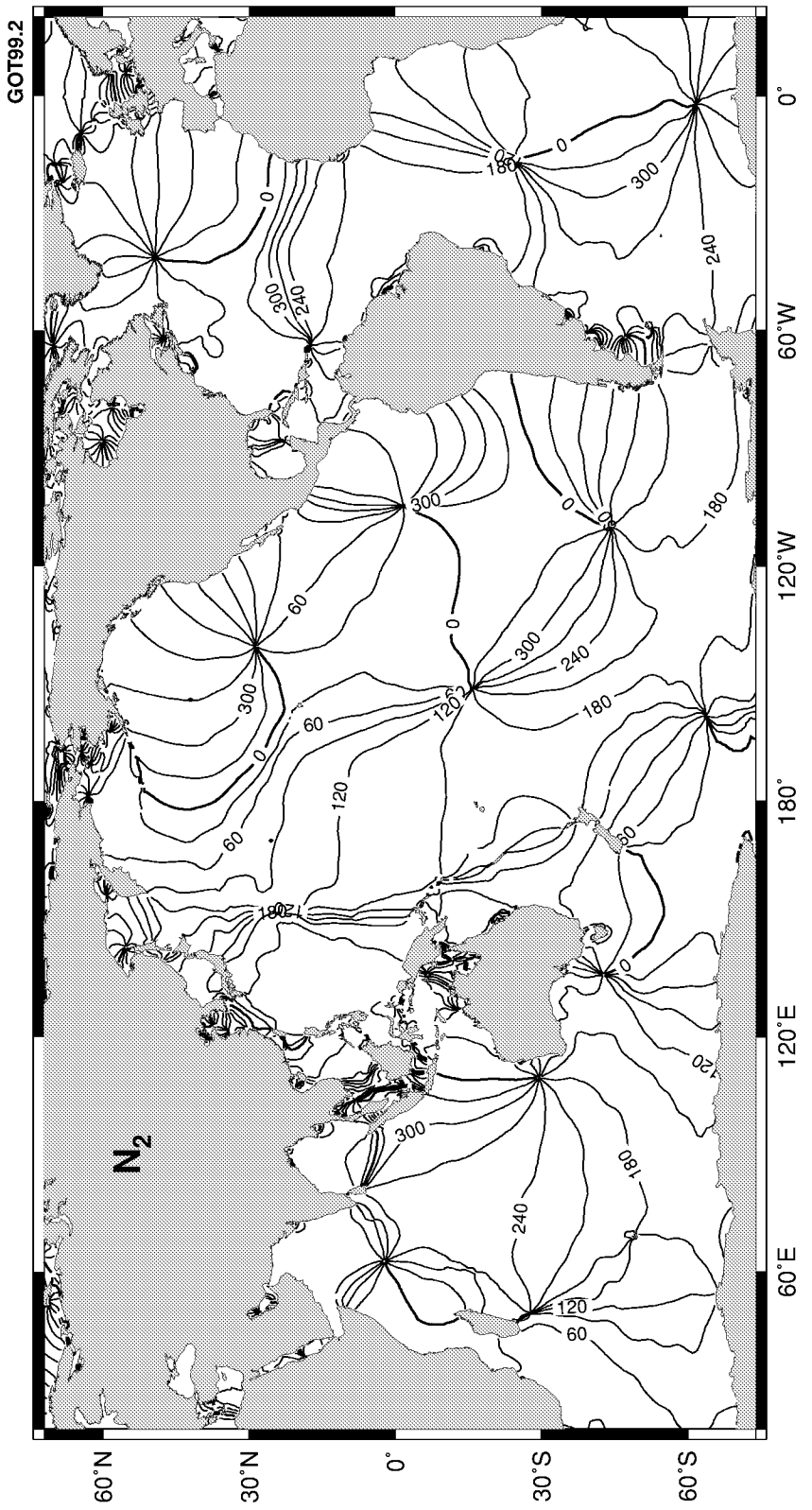

Figure A10. Greenwich phase lag of N_2 tide. Contour interval = 30˚.

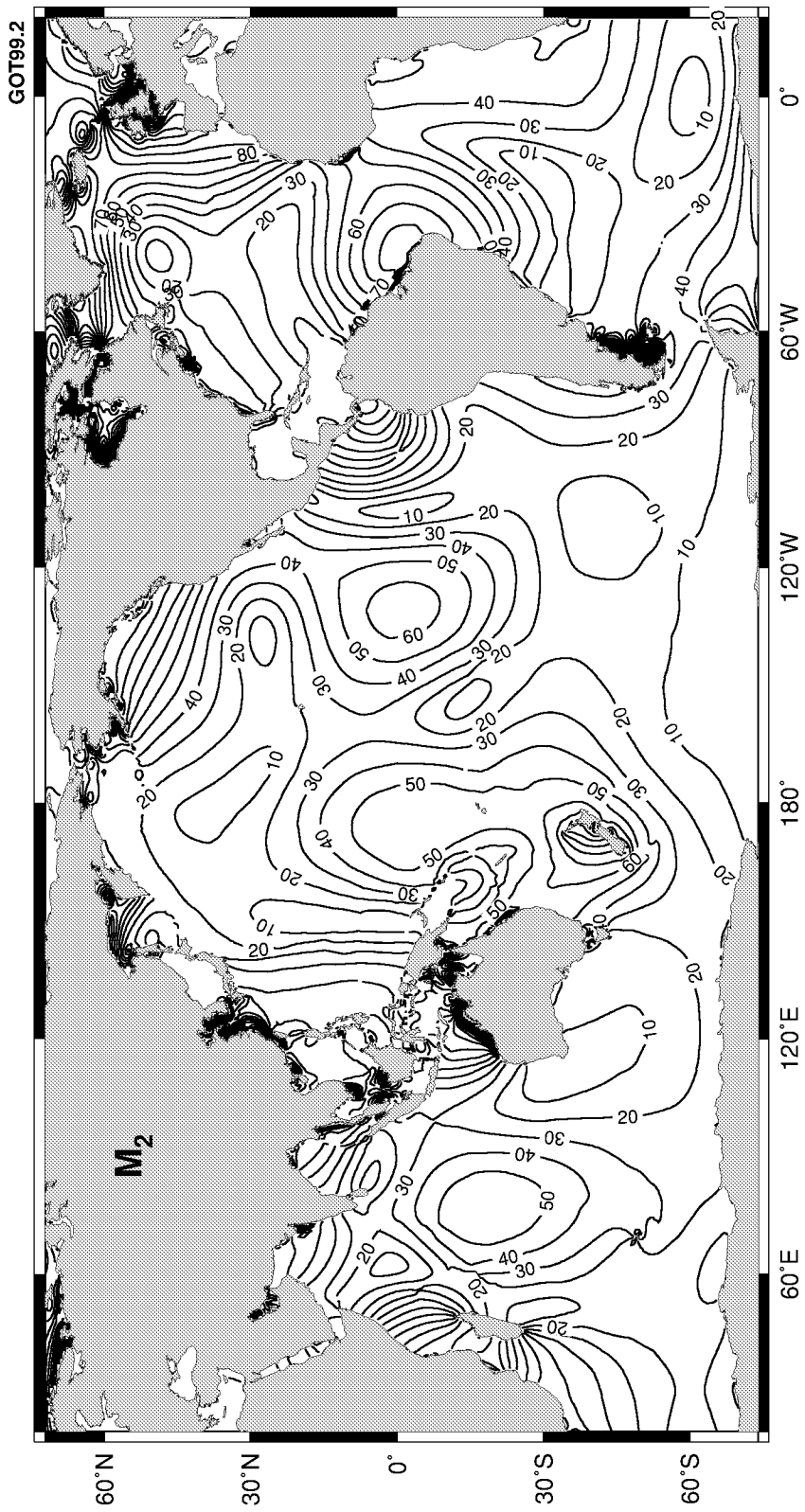

Figure A11. Amplitude of M_2 tide. Contour interval = 10 cm.

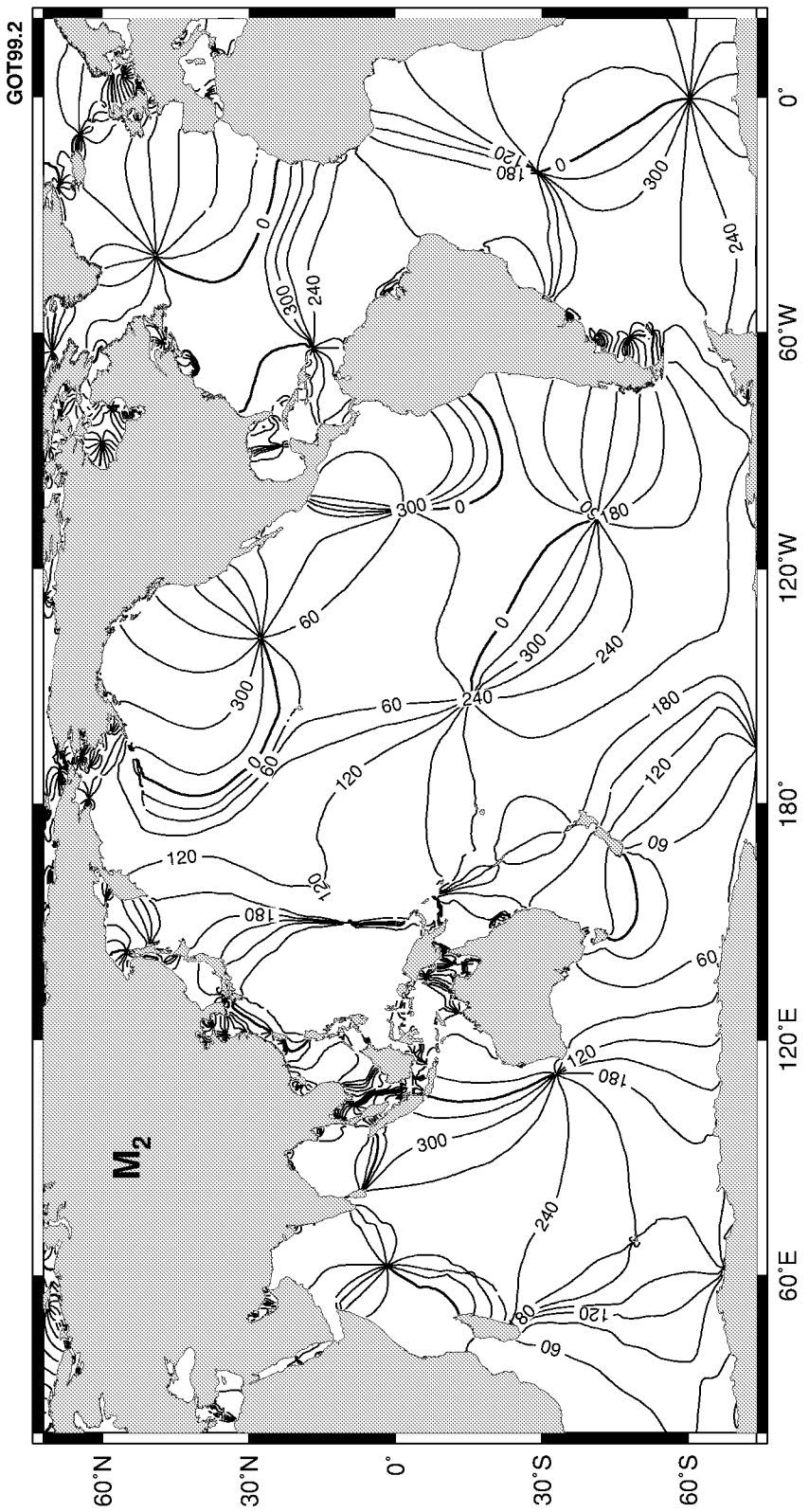

Figure A12. Greenwich phase lag of M_2 tide. Contour interval = 30°.

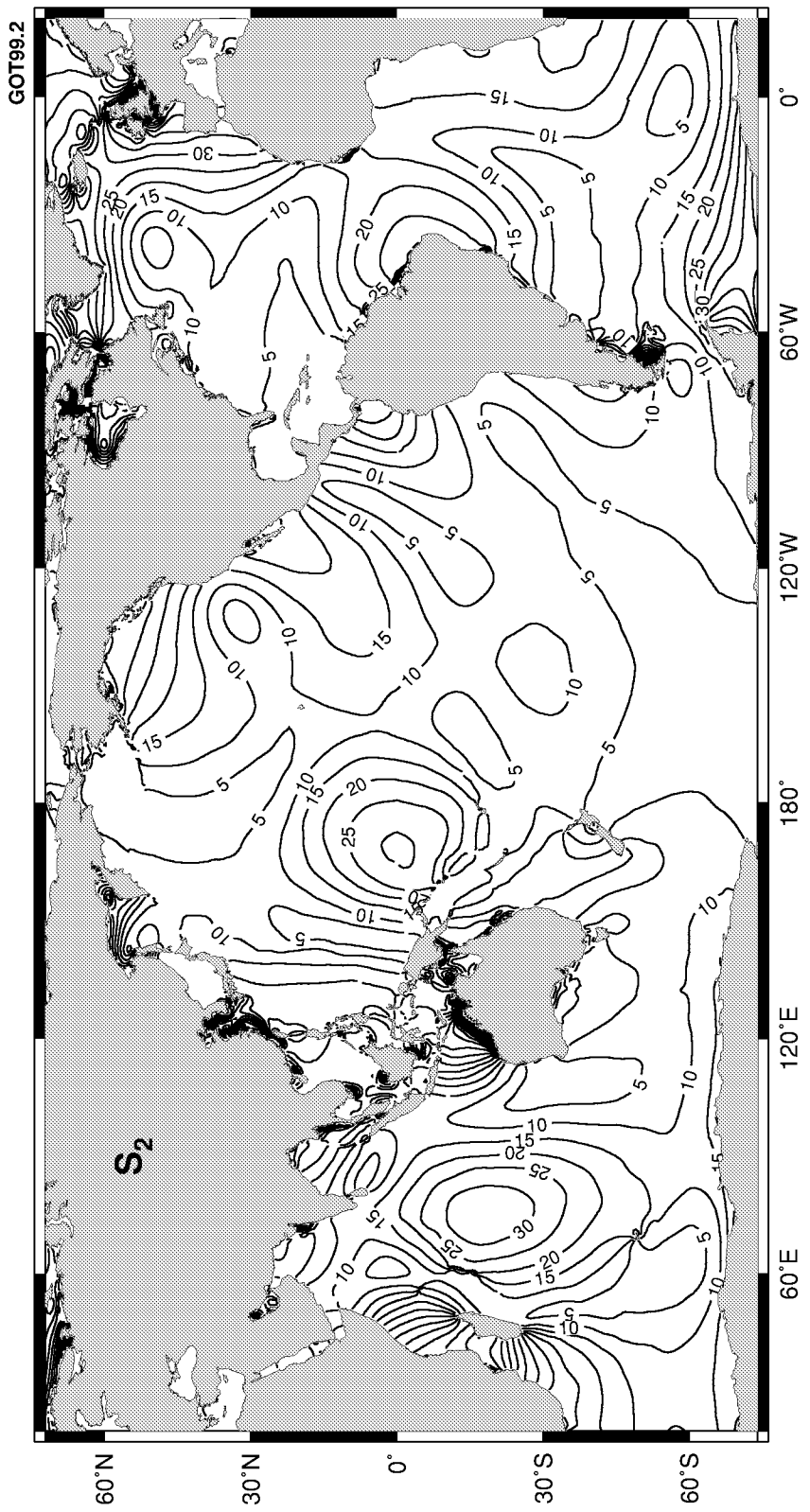

Figure A13. Amplitude of S_2 tide. Contour interval = 5 cm.

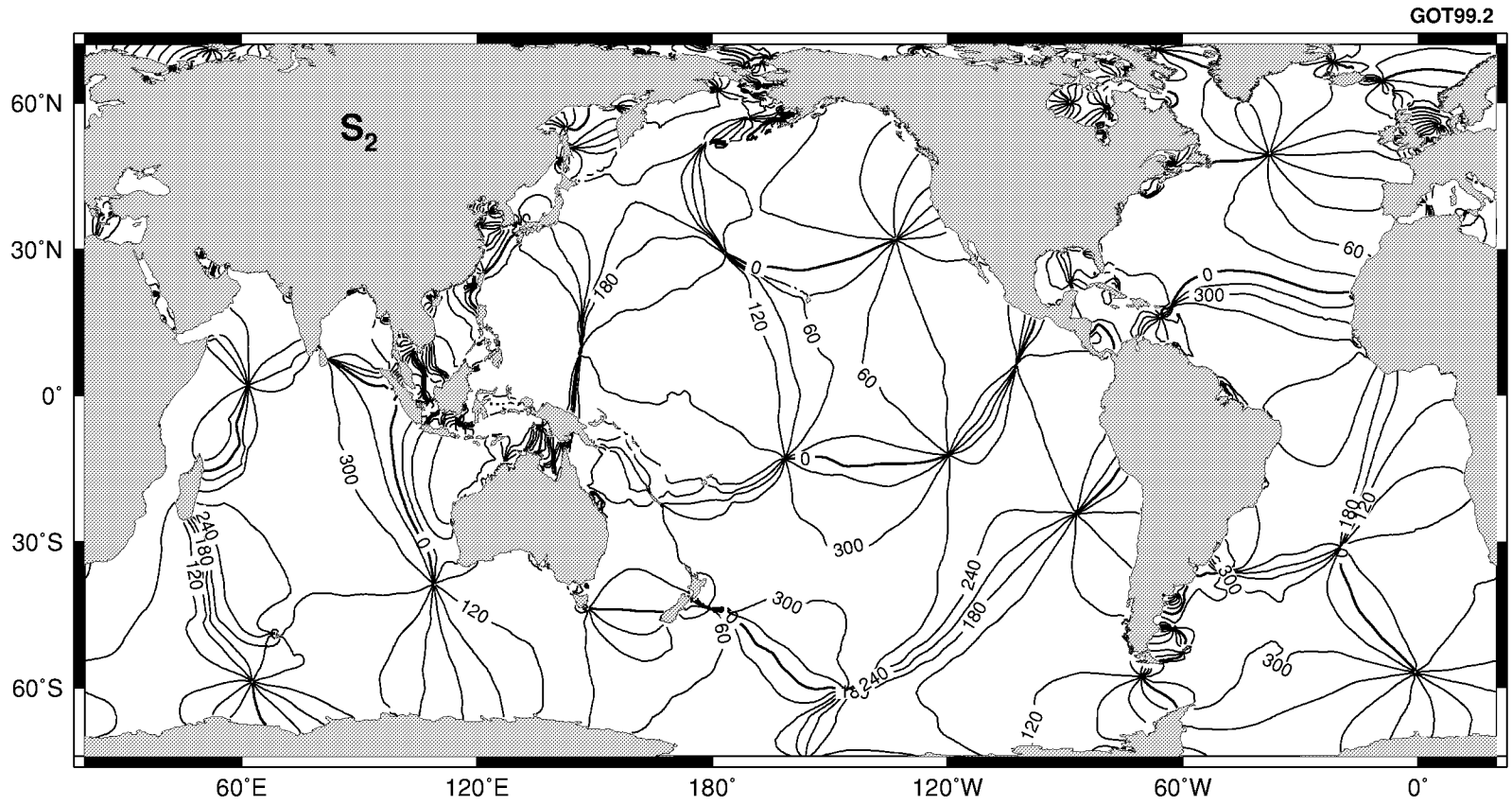

Figure A14. Greenwich phase lag of S_2 tide. Contour interval = 30˚.

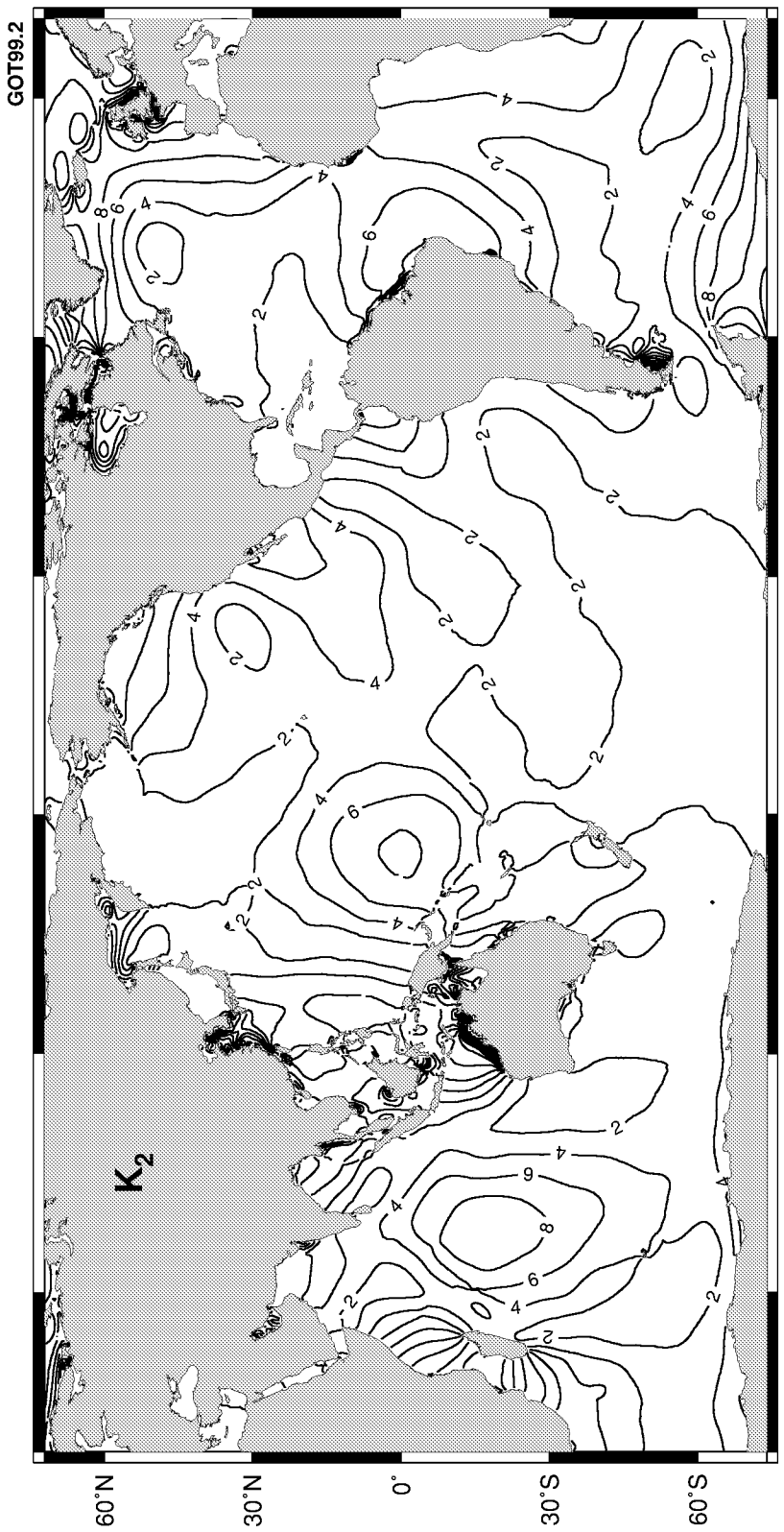

Figure A15. Amplitude of K_2 tide. Contour interval = 2 cm.

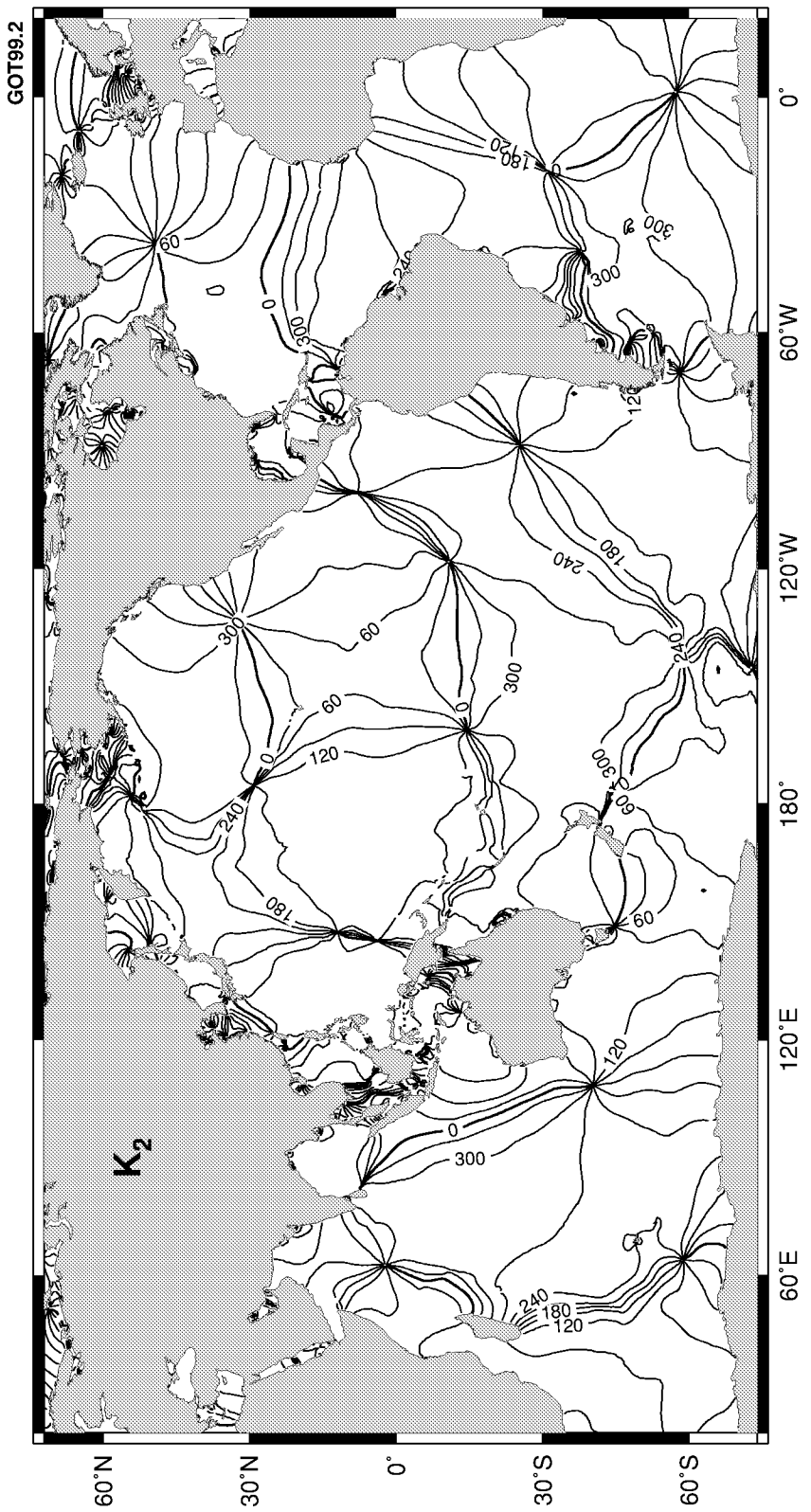

Figure A16. Greenwich phase lag of K_2 tide. Contour interval = 30°.

B Global Ocean Loading Charts for M_2

Deformation of the Earth by ocean tidal loading affects a wide range of modern geodetic measurements. Thus, one important application of global tide models such as the present one is to predict such deformations. The predictions can be used either to correct geodetic measurements for the ocean effect or to compare theoretical predictions with direct observations.

The following pages display global load-tide charts corresponding to several different types of geodetic measurements, for the M_2 tide. Already discussed in this report is the radial displacement; correction for that plays a crucial role in obtaining a purely oceanic tide from altimeter measurements. Similar charts are given for horizontal displacements, both northward and eastward. Together, these three components of displacement must be accounted for in precise positioning, including the positioning of satellite tracking stations. Similar charts are given for the effect of ocean tides on gravimetry measurements and for the self-attraction/loading effect on the hydrodynamical forcing of tides.

All of these calculations are based on high-degree spherical harmonic expansions of the ocean tide. Similar calculations could be performed with various kernel (or Green's) functions. In fact, several types of deformations (e.g., tidal tilt) generally require the higher spatial resolutions inherent in the kernel-function approach, but the quantities shown here appear to be sufficiently accurate when using high-degree (n = 360) spherical harmonics. A notable exception is any geodetic station very near an ocean coastline, which can be sensitive to the precise ocean-land boundary; such stations normally require special local tide models of high spatial resolution. Moreover, one should remember that these are gross-earth calculations of "homogeneous" deformations and that it is possible that local geological effects could cause perturbations in some regions. Such local effects are commonplace for tidal tilt measurements (e.g., the "cavity effect"). I am aware of no evidence showing significant effects in radial or horizontal displacement, although some theoretical finite-element calculations of very localized areas have suggested effects as large as about 10%. Local effects in gravity have been alleged, but the interpretations are controversial.

The charts of this section follow from the following equations. More extensive discussions may be found in geodesy texts. All loading coefficients h'_n, k'_n, l'_n are adopted from *Farrell* (1972). Other coefficient sets based on more modern Earth models have been published since Farrell's work, but the differences are small and appear to have little significant effect on the final results. (The core resonance effect near K_1, with perturbations primarily in h'_2, etc., is also evidently small enough to neglect in loading calculations at present levels of accuracy.)

Let the ocean tidal elevation ζ be decomposed into spherical harmonics of form

$$\zeta = \sum_{n,m} a_n Y_n^m. \tag{B.1}$$

where for the calculations here n is taken from 1 to 360. The the vertical displace-

ment induced by tidal loading can be calculated from

$$r_{\text{up}} = \sum_{n,m} \alpha_n h'_n a_n Y_n^m, \tag{B.2}$$

where

$$\alpha_n = \frac{\rho_w}{\rho_e} \frac{3}{2n+1}$$

with ρ_e = 5518 kg m^{-3} the mean density of the Earth and ρ_w = 1035 kg m^{-3} the mean density of seawater. Similarly, the horizontal displacements are given by

$$r_{\text{east}} = \sum_{n,m} \alpha_n l'_n a_n \frac{\partial Y_n^m}{\sin\theta \, \partial\phi} \tag{B.3}$$

$$r_{\text{north}} = -\sum_{n,m} \alpha_n l'_n a_n \, \partial Y_n^m / \partial\theta. \tag{B.4}$$

The effect of ocean tidal self-attraction and loading on the dynamics of the tide, which must be accounted for in numerical hydrodynamic models is given by (e.g., *Ray,* 1998)

$$\Upsilon = \sum_{n,m} (1 + k'_n - h'_n) \, \alpha_n \, a_n \, Y_n^m \tag{B.5}$$

where the effect is expressed in length units, similar to the tidal elevation. Finally the effect on gravity observations can be written (*Merriam*, 1980)

$$\Delta g = \sum_{n,m} -g\{1/2 + (n+1)k'_n - 2h'_n\} \, \alpha_n \, a_n \, Y_n^m / a_e \tag{B.6}$$

with a_e the mean Earth radius. The charts that follow display all these ocean-loading effects in terms of an amplitude and a Greenwich phase lag.

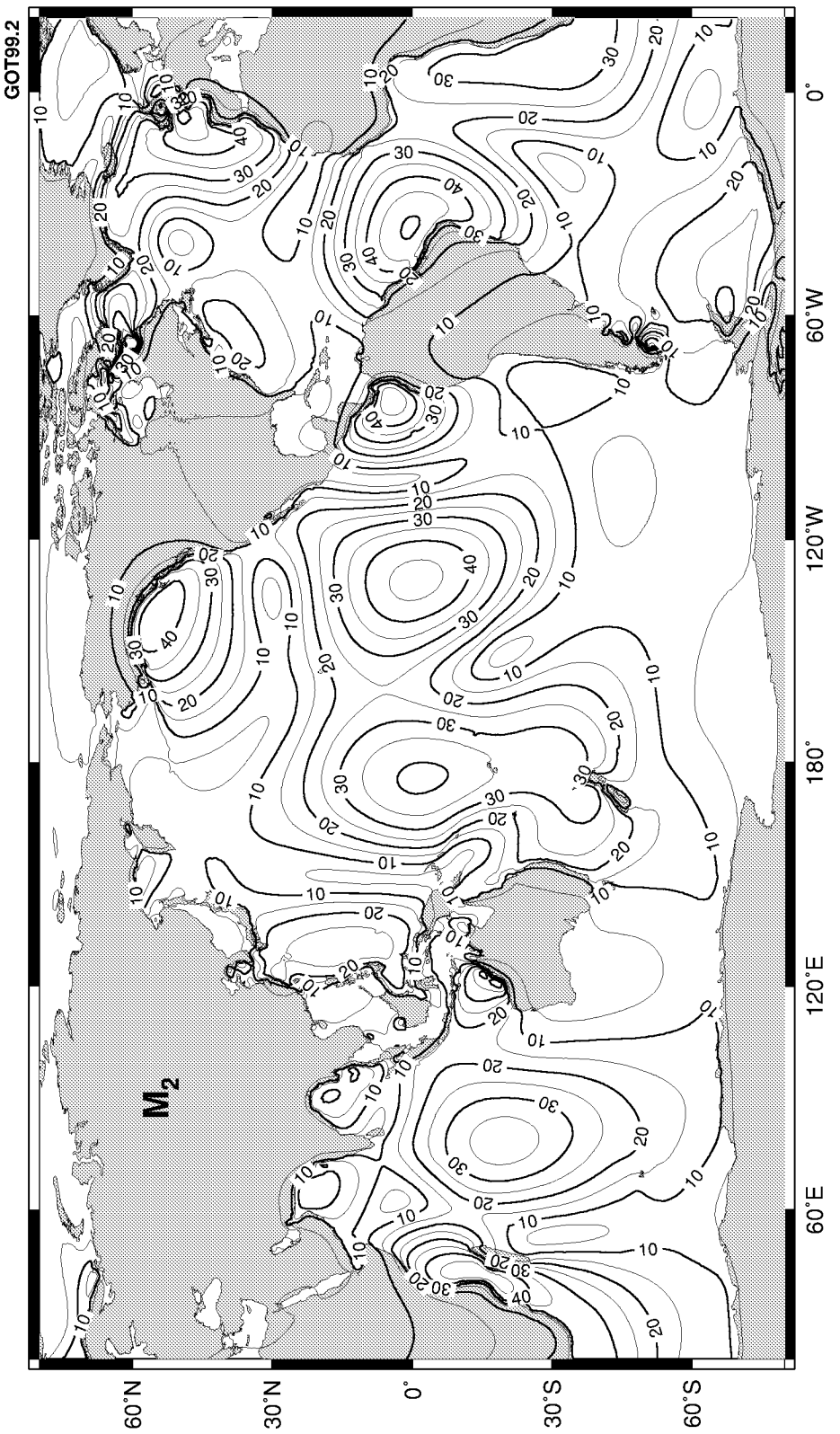

Figure B1. Amplitude of M_2 vertical displacement load tide. Contour interval = 5 mm.

Figure B2. Greenwich phase lag of M_2 vertical displacement load tide. Contour interval = 30°.

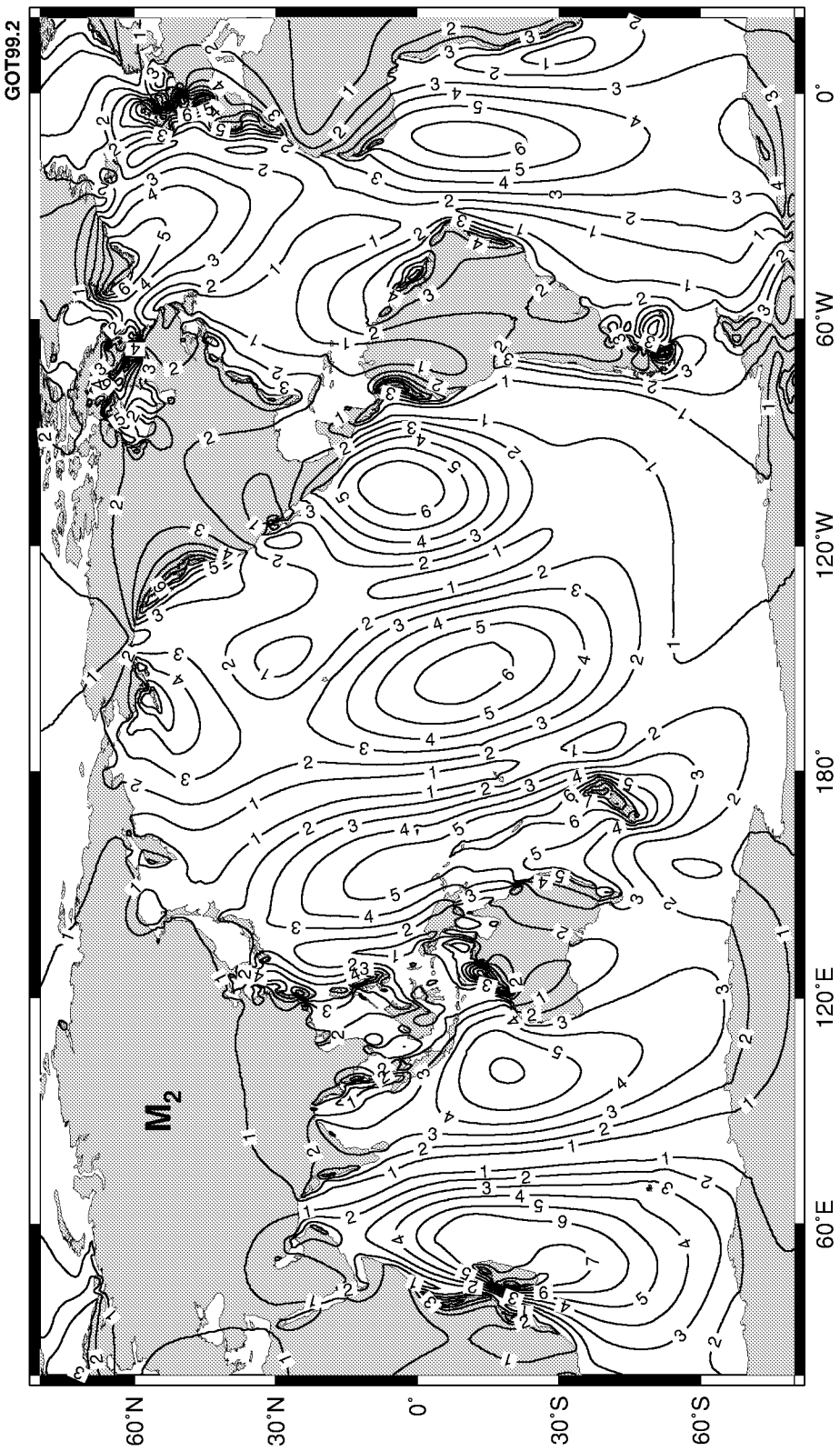

Figure B3. Amplitude of M_2 eastward displacement load tide. Contour interval = 1 mm.

Figure B4. Greenwich phase lag of M_2 eastward displacement load tide. Contour interval = 30°.

Figure B5. Amplitude of M_2 northward displacement load tide. Contour interval = 1 mm.

Figure B6. Greenwich phase lag of M_2 northward displacement load tide. Contour interval = 30˚.

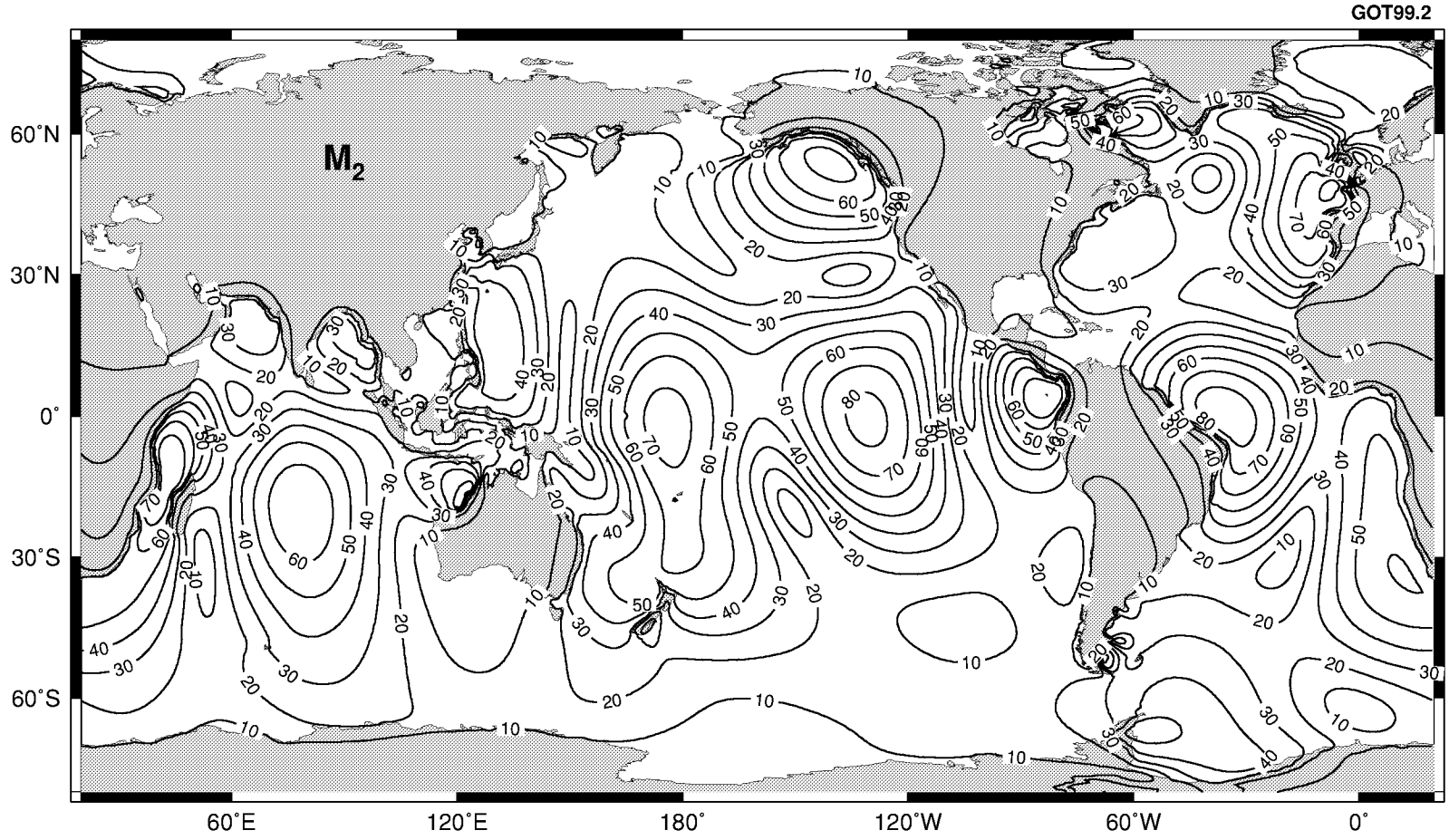

Figure B7. Amplitude of M_2 self-attraction/loading "tide". Contour interval = 10 mm.

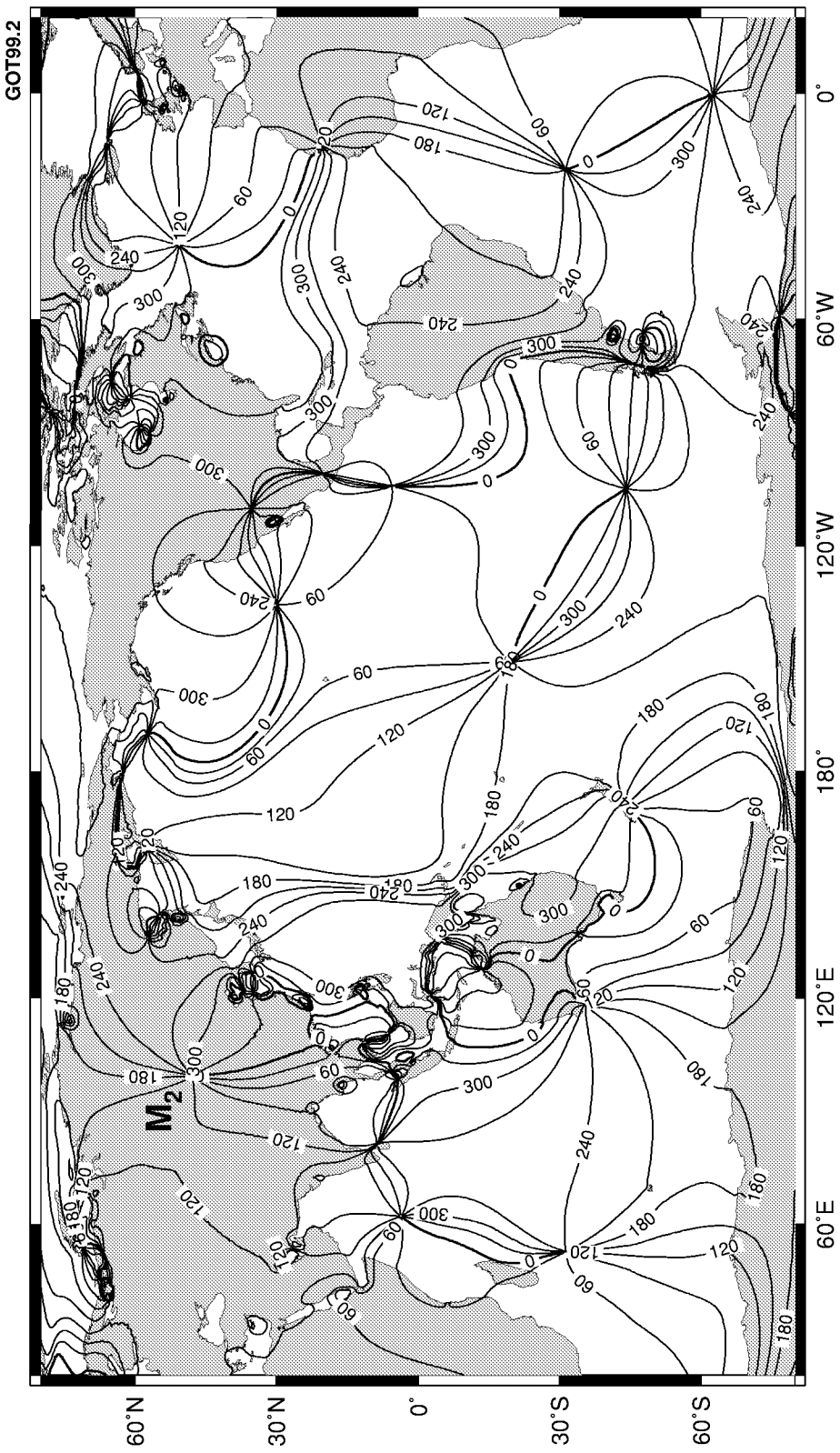

Figure B8. Greenwich phase lag of M_2 self-attraction/loading "tide". Contour interval = 30°.

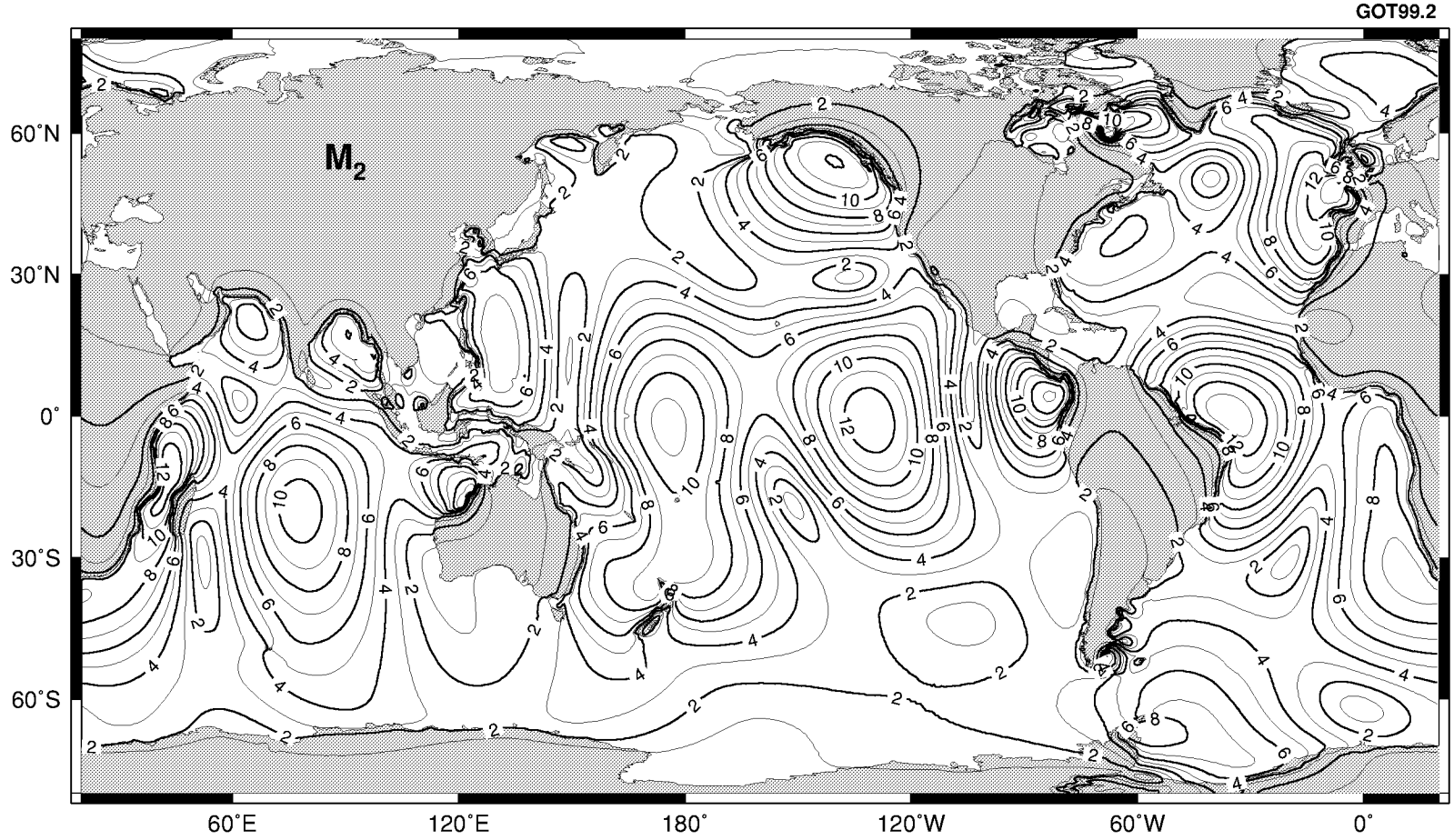

Figure B9. Amplitude of M_2 ocean-tide gravimetric effect. Contour interval = 1 microgals.

Figure B10. Greenwich phase lag of M_2 ocean-tide gravimetric effect. Contour interval = 30˚.

C Global Charts of Tidal Transport Ellipses

The following charts show M_2, S_2, O_1, and K_1 barotropic current ellipses, which have been deduced from the tidal elevations described above. These ellipses are strictly volume transports (velocity $\times$ depth), which are similar to velocity ellipses but less dominated by extreme amplitudes over shelf regions. For each ellipse the radial arm indicates the direction and magnitude of transport at the time of zero tidal argument (e.g., at Greenwich lunar transit for M_2); the continuous part of the ellipse then sweeps out the transport vector for the remainder of the tidal cycle, thereby also showing the sense of rotation. For display purposes the ellipses have been plotted every 5° over the globe, but the original data reside on the same 0.5° grid as the elevation solutions.

The tidal transports have been deduced from the elevations by solving the linearized two-dimensional momentum equations and the continuity equation as a large-scale sparse least-squares problem. The momentum equations include a linearized bottom-friction dissipation term and rigorously computed self-attraction and loading terms (according to Equation B.5). Further details of these calculations, as well as comparisons of the resulting current velocities with *in situ* measurements derived from either moored current meters or acoustic transmission arrays, are given elsewhere (*Ray*, 1999).

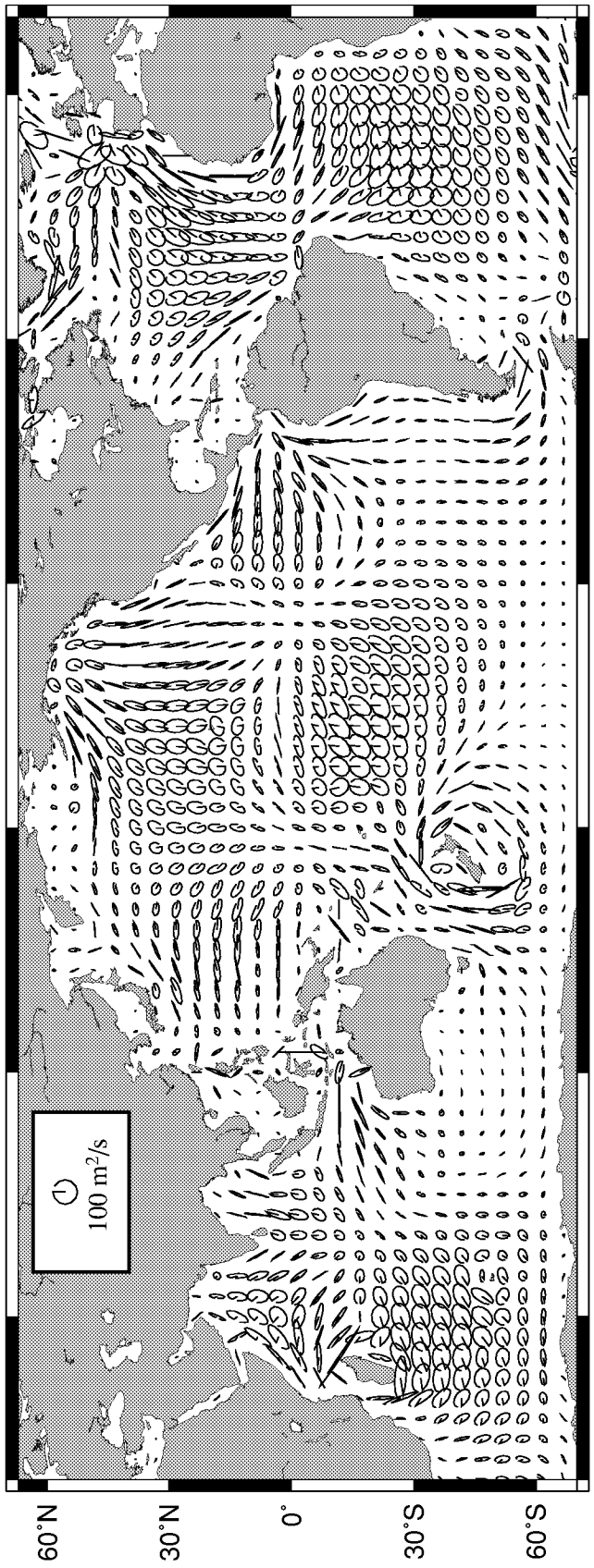

Figure C1. Volume transport ellipses for M_2.

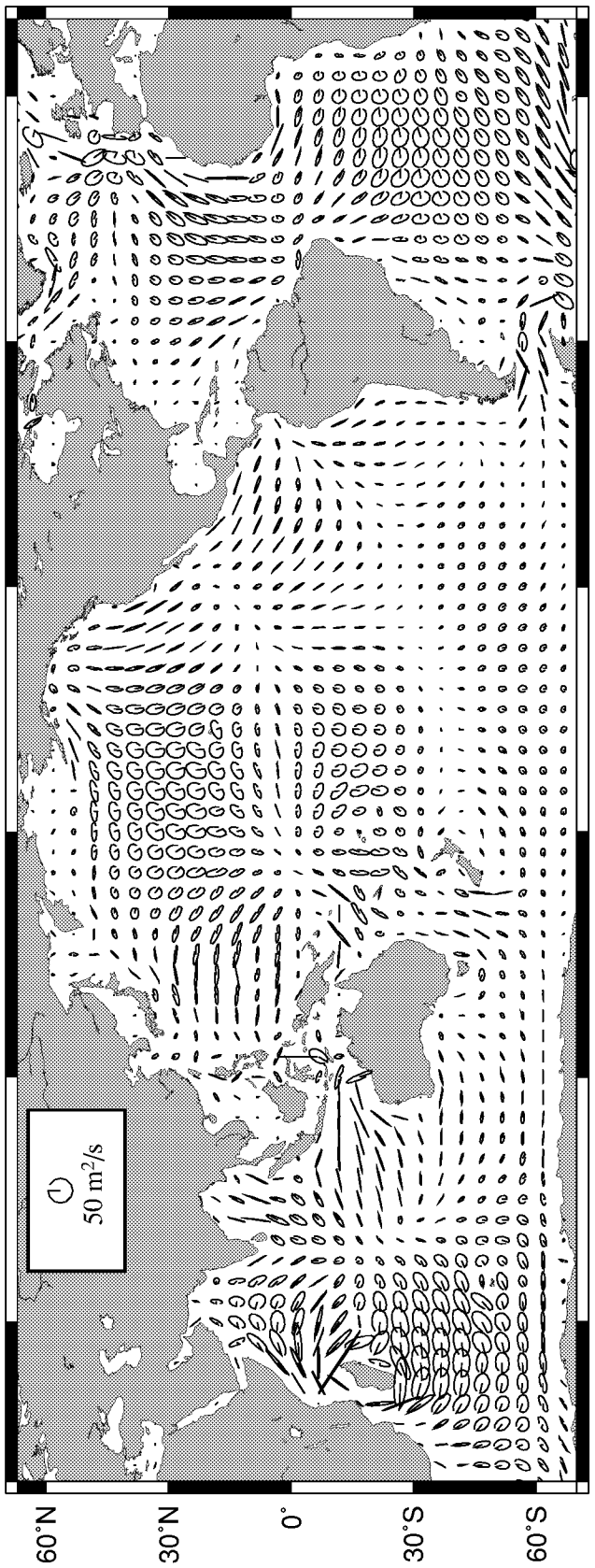

Figure C2. Volume transport ellipses for S_2.

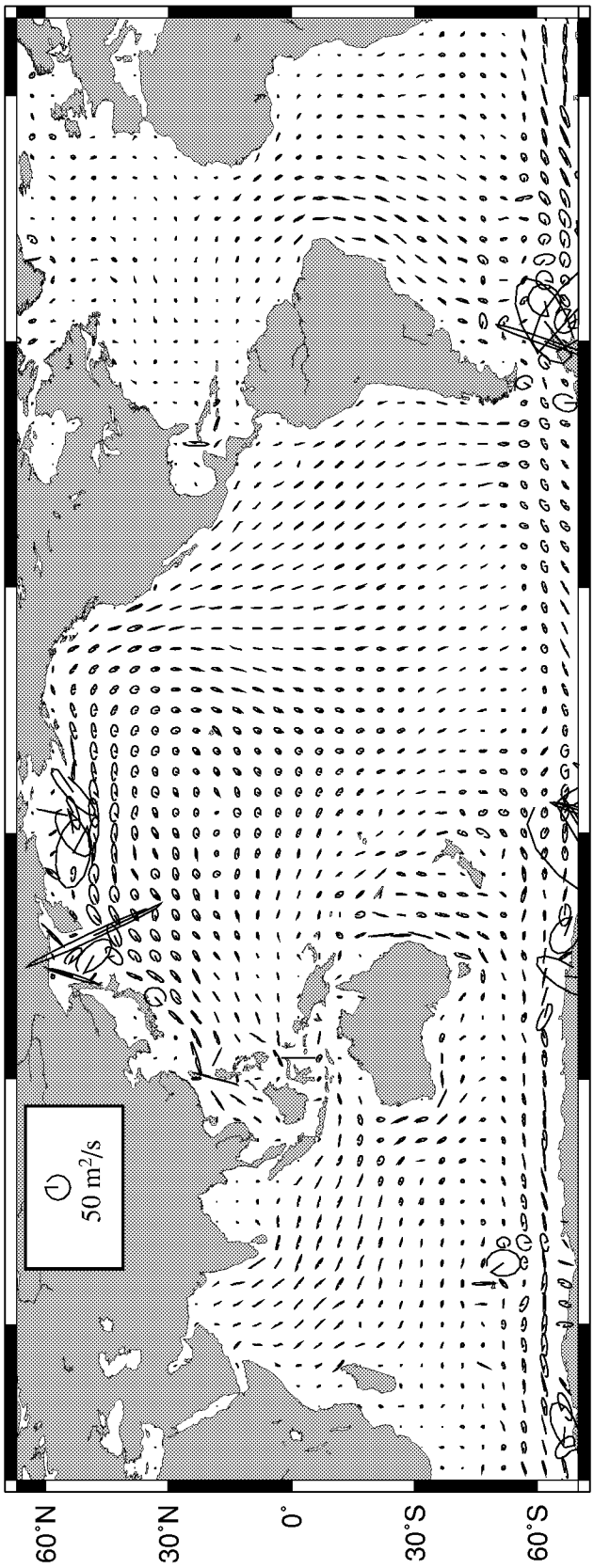

Figure C3. Volume transport ellipses for O_1.

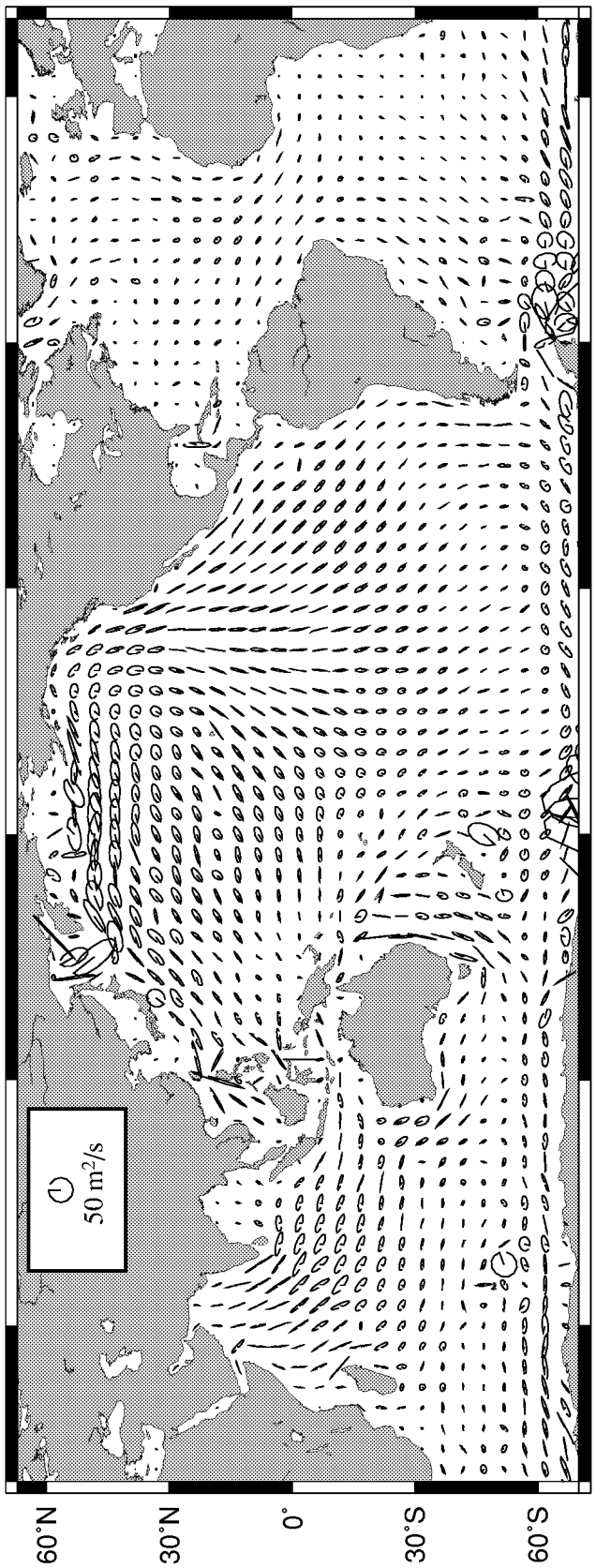

Figure C4. Volume transport ellipses for K_1.

REFERENCES

Andersen, O. B., P. L. Woodworth, and R. A. Flather, Intercomparison of recent ocean tide models, *Journal of Geophysical Research,* **100**, 25261–25282, 1995.

Cartwright, D. E. and A. C. Edden, Corrected tables of tidal harmonics, *Geophysical Journal of the Royal Astronomical Society,* **33**, 253–264, 1973.

Cartwright, D. E. and R. D. Ray, Oceanic tides from Geosat altimetry, *Journal of Geophysical Research,* **95**, 3069–3090, 1990.

Cartwright, D. E. and R. D. Ray, Energetics of global ocean tides from Geosat altimetry, *Journal of Geophysical Research,* **96**, 16897–16912, 1991.

Cartwright, D. E. and R. D. Ray, On the radiational anomaly in the global ocean tide with reference to satellite altimetry, *Oceanologica Acta*, **17**, 453–459, 1994.

Cartwright, D. E., R. D. Ray, and B. V. Sanchez, Oceanic tide maps and spherical harmonic coefficients from Geosat altimetry, NASA Tech. Memo. 104544, Goddard Space Flight Center, Greenbelt, 74 pp., 1991.

Cartwright, D. E. and R. J. Tayler, New computations of the tide-generating potential, *Geophysical Journal of the Royal Astronomical Society,* **23**, 45–73, 1971.

Desai, S. D. and J. M. Wahr, Empirical ocean tide models estimated from TOPEX/POSEIDON altimetry, *Journal of Geophysical Research,* **100**, 25205–25228, 1995.

Doodson, A. T. and H. D. Warburg, *Admiralty Manual of Tides,* HMSO, 1941.

Farrell, W. E., Deformation of the Earth by surface loads, *Reviews of Geophysics and Space Physics,* **10**, 761–797, 1972.

Greenberg, A. D., A numerical model investigation of tidal phenomena in the Bay of Fundy and Gulf of Maine, *Marine Geodesy,* **2**, 161–187, 1979.

Hsu, H.-H. and B. J. Hoskins, Tidal fluctuations as seen in ECMWF data, *Quarterly Journal of the Royal Meteorological Society*, **115**, 247–264, 1989.

Koblinsky, C. J., B. D. Beckley, R. D. Ray, Y.-M. Wang, L. Tsaoussi, A. Brenner, R. Williamson, NASA Ocean Altimeter Pathfinder Project—Report 1: Data Processing Handbook, NASA Tech. Memo. 208605, 55 pp., 1999.

Lambeck, K., *Geophysical Geodesy,* Cambridge Univ. Press, 1988.

Lambert, A., S. D. Pagiatakis, A. P. Billyard, H. Dragert, Improved ocean tide loading corrections for gravity and displacement: Canada and northern United States, *Journal of Geophysical Research,* **103**, 30231–30244, 1998.

Le Provost, C., M. L. Genco, F. Lyard, P. Vincent, P. Canceil, Spectroscopy of the world ocean tides from a finite element hydrodynamic model, *Journal of Geophysical Research,* **99**, 24777–24797.

Le Provost, C., F. Lyard, J.-M. Molines, M. L. Genco, F. Rabilloud, A hydrodynamic ocean tide model improved by assimilating a satellite altimeter-derived data set, *Journal of Geophysical Research,* **103**, 5513–5529, 1998.

Lerch, F. J. et al. Geopotential models of the Earth from satellite tracking, altimeter and surface gravity observations: GEM-T3 and GEM-T3S, NASA Tech. Memo. 104555, Goddard Space Flight Center, 118 pp., 1992.

Marshall, J. A., N. P. Zelensky, S. M. Klosko, D. S. Chinn, S. B. Luthcke, K. E. Rachlin, R. G. Williamson, The temporal and spatial characteristics of the TOPEX/POSEIDON radial orbit error, *Journal of Geophysical Research,* **100**, 25331–25352, 1995.

Merriam, J. B., The series computation of the gravitational perturbation due to an ocean tide, *Physics of the Earth and Planetary Interiors,* **23**, 81–86, 1980.

Munk, W. H. and D. E. Cartwright, Tidal spectroscopy and prediction, *Philosophical Transactions of the Royal Society of London,* **A259**, 533–581, 1966.

Munk, W. H., B. Zetler, and G. W. Groves, Tidal cusps, *Geophysical Journal*, **10**, 211–219, 1965.

Proctor, R., R. A. Flather, and A. J. Elliott, Modeling tides and surface drift in the Arabian Gulf—application to the Gulf oil spill, *Continental Shelf Research,* **14**, 531–545, 1994.

Ray, R. D., Ocean self-attraction and loading in numerical tidal models, *Marine Geodesy*, **21**, 181–192, 1998.

Ray, R. D., Inversion of oceanic tidal currents from measured elevations, submitted for publication, 1999.

Ray, R. D. and G. T. Mitchum, Surface manifestation of internal tides in the deep ocean: observations from altimetry and island gauges, *Progress in Oceanography,* **40**, 135–162, 1997.

Ray, R. D., B. Sanchez, D. E. Cartwright, Some extensions of the response method of tidal analysis applied to Topex/Poseidon (abstract), *Eos, Trans. AGU,* **75** (16), Spring Meet. Suppl., 108, 1994.

Schrama, E. J. O. and R. D. Ray, A preliminary tidal analsis of TOPEX/POSEIDON altimetry, *Journal of Geophysical Research,* **99**, 24799–24808.

Shum, C. K., P. L. Woodworth, O. B. Andersen, G. Egbert, O. Francis, C. King, S. Klosko, C. Le Provost, X. Li, J.-M. Molines, M. Parke, R. Ray, M. Schlax, D. Stammer, C. Tierney, P. Vincent, C. Wunsch, Accuracy assessment of recent ocean tide models, *Journal of Geophysical Research,* **102**, 25173–25194, 1997.

Smith, A. J. E. and O. B. Andersen, Errors in recent ocean tide models: possible origin and cause, *Progress in Oceanography,* **40**, 325–336, 1997.

Stammer, D., C. Wunsch, and R. Ponte, De-aliasing of global high frequency barotropic motions in altimeter observations, *Geophysical Research Letters,* in press, 1999.

Tapley, B. D., M. M. Watkins, J. C. Ries, G. Davis, R. J. Eanes, H. J. Rim, B. E. Schutz, C. K. Shum, R. S. Nerem, F. J. Lerch, J. A. Marshall, S. M. Klosko, N. K. Pavlis, R. G. Williamson, The Joint Gravity Model 3, *Journal of Geophysical Research,* **101**, 28029–28049, 1996.

Wahr, J. M., Body tides on an elliptical, rotating, elastic and oceanless earth, *Geophysical Journal of the Royal Astronomical Society,* **64**, 677–703, 1981.

REPORT DOCUMENTATION PAGE

Form Approved
OMB No. 0704-0188

1. AGENCY USE ONLY *(Leave blank)*	2. REPORT DATE	3. REPORT TYPE AND DATES COVERED
	September 1999	TM—1999–209478

4. TITLE AND SUBTITLE
A Global Ocean Tide Model From TOPEX/POSEIDON Altimetry: GOT99.2

5. FUNDING NUMBERS
926

6. AUTHOR(S)
Ray, R.D.

7. PERFORMING ORGANIZATION NAME(S) AND ADDRESS (ES)
Laboratory for Terrestrial Physics
Space Geodesy Branch
Goddard Space Flight Center
Greenbelt, Maryland 20771

8. PEFORMING ORGANIZATION REPORT NUMBER
99B00073

9. SPONSORING / MONITORING AGENCY NAME(S) AND ADDRESS (ES)
National Aeronautics and Space Administration
Washington, DC 20546-0001

10. SPONSORING / MONITORING AGENCY REPORT NUMBER
TM—1999–209478

11. SUPPLEMENTARY NOTES

12a. DISTRIBUTION / AVAILABILITY STATEMENT
Unclassified–Unlimited
Subject Category: 48
Report available from the NASA Center for AeroSpace Information,
7121 Standard Drive, Hanover, MD 21076-1320. (301) 621-0390.

12b. DISTRIBUTION CODE

13. ABSTRACT *(Maximum 200 words)*

Goddard Ocean Tide model GOT99.2 is a new solution for the amplitudes and phases of the global oceanic tides, based on over six years of sea-surface height measurements by the TOPEX/POSEIDON satellite altimeter. Comparison with deep-ocean tide-gauge measurements show that this new tidal solution is an improvement over previous global models, with accuracies for the main semidiurnal lunar constituent M_2 now below 1.5 cm (deep water only). The new solution benefits from use of prior hydrodynamic models, several in shallow and inland seas as well as the global finite-element model FES94.1. This report describes some of the data processing details involved in handling the altimetry, and it provides a comprehensive set of global cotidal charts of the resulting solutions. Various derived tidal charts are also provided, including tidal loading deformation charts, tidal gravimetric charts, and tidal current velocity (or transport) charts. Finally, low-degree spherical harmonic coefficients are computed by numerical quadrature and are tabulated for the major short-period tides; these are useful for a variety of geodetic and geophysical purposes, especially in combination with similar estimates from satellite laser ranging.

14. SUBJECT TERMS
TOPEX/POSEIDON; global oceanic tides; sea-surface height measurements.

15. NUMBER OF PAGES
58

16. PRICE CODE

17. SECURITY CLASSIFICATION OF REPORT	18. SECURITY CLASSIFICATION OF THIS PAGE	19. SECURITY CLASSIFICATION OF ABSTRACT	20. LIMITATION OF ABSTRACT
Unclassified	Unclassified	Unclassified	UL